Article

Molecular Control of Macroscopic Cubic, Columnar, and Lamellar Organizations in Luminescent Lanthanide-Containing Thermotropic Liquid Crystals

Emmanuel Terazzi, Stphane Torelli, Grald Bernardinelli, Jean-Pierre Rivera, Jean-Marc Bnech, Cyril Bourgogne, Bertrand Donnio, Daniel Guillon, Daniel Imbert, Jean-Claude G. Bnzli, Andr Pinto, Damien Jeannerat, and Claude Piguet

J. Am. Chem. Soc., **2005**, 127 (3), 888-903• DOI: 10.1021/ja0446101 • Publication Date (Web): 30 December 2004

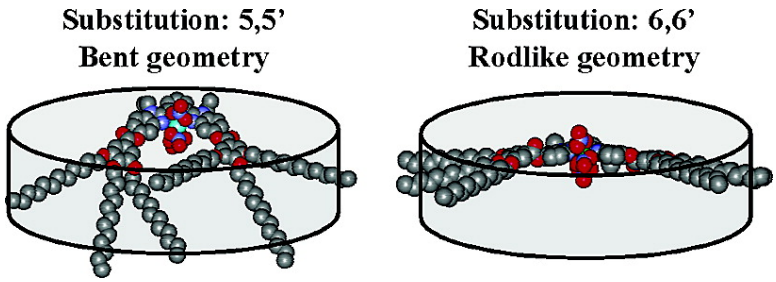

More About This Article

Additional resources and features associated with this article are available within the HTML version:

- Supporting Information
- Links to the 21 articles that cite this article, as of the time of this article download
- Access to high resolution figures
- Links to articles and content related to this article
- Copyright permission to reproduce figures and/or text from this article

View the Full Text HTML

J|A|C|S
ARTICLES
Published on Web 12/30/2004

Molecular Control of Macroscopic Cubic, Columnar, and Lamellar Organizations in Luminescent Lanthanide-Containing Thermotropic Liquid Crystals

Emmanuel Terazzi,[†] Stéphane Torelli,[†] Gérald Bernardinelli,[‡] Jean-Pierre Rivera,[†] Jean-Marc Bénech,[†] Cyril Bourgogne,[§] Bertrand Donnio,[§] Daniel Guillon,[§] Daniel Imbert,[⊥] Jean-Claude G. Bünzli,[⊥] André Pinto,[∥] Damien Jeannerat,[∥] and Claude Piguet*,[†]

Contribution from the Department of Inorganic, Analytical and Applied Chemistry, and Department of Organic Chemistry, University of Geneva, 30 quai E. Ansermet, CH-1211 Geneva 4, Switzerland, Laboratory of X-ray Crystallography, University of Geneva, 24 quai E. Ansermet, CH-1211 Geneva 4, Switzerland, Ecole Polytechnique Fédérale de Lausanne, Laboratory of Lanthanide Supramolecular Chemistry, BCH 1402, CH-1015 Lausanne, Switzerland, and Institut de Physique et Chimie des Matériaux de Strasbourg-IPCMS, Groupe des Matériaux Organiques, 23 rue du Loess, B.P. 43, F-67034 Strasbourg Cedex 2, France

Received September 6, 2004; E-mail: Claude.Piguet@chiam.unige.ch

Abstract: The connection of lipophilic gallic acid derivatives at the 5,5′- or 6,6′-positions of the rigid 2,6-bis(1-ethyl-benzimidazol-2-yl)pyridine core provides two pro-mesogenic tridentate ligands **L10** and **L12**, whose molecular shapes, anisometries, and directional intermolecular π-stacking can be tuned. X-ray diffraction data in the crystalline state, combined with solution ^{1}H NMR measurements, show that complexation with trivalent lanthanides, Ln(III), produces the neutral hemi-disklike complexes [Ln(**L*i***)$(NO_3)_3$] ($i = 10, 12$), which dimerize to give the rodlike bimetallic complexes [Ln_2(**L*i***)$_2(NO_3)_6$] at lower temperature. The relevant thermodynamic parameters for the latter process depend on the nature of the ligand, the size of the metal ion, and the strength of the intermolecular interactions involved in the condensed phase. These three-dimensional models obtained for the complexes in the crystals and in solution are eventually confronted with small-angle XRD profiles recorded in the intermediate thermotropic liquid crystalline phase, in which the rigidity of the packed polyaromatic cores is maintained, while the alkyl chains are molten. According to the specific geometries and nuclearities of the molecular complexes, three types of mesophases (lamellar, columnar, and cubic) can be induced, which provides a direct correlation between the microscopic arrangements and the macroscopic ordering in lanthanide-containing metallomesogens.

Introduction

The design of thermotropic metallomesogens, that is, metal-containing liquid crystals, obeys the same rules as those established for the preparation of mesophases with organic molecules.[1] A thermally induced microsegregation between the flexible alkyl chains (large melting entropy and small melting enthalpy)[2] and the rigid organometallic core (large melting enthalpy and small melting entropy)[3] is thus required for the generation of a mesophase occurring between the crystalline and isotropic liquid states.[1] Lipophilic complexes possessing rigid *rodlike* cores (i.e., in which the axial component is larger than the radial component) thus produce mesophases with nematic (orientational order without positional order) or smectic (orientational order with one-dimensional positional order) organization, while those with rigid disklike cores (i.e., in which the radial component is larger than the axial component) lead to nematic and columnar mesophases (two-dimensional arrangements of the columns). Specific molecular shapes mainly result from the global anisometry of the ligands, but the stereochemical preferences of the metal ions also contribute to the three-dimensional architectures.[1] Except for the special case of ferrocene, in which "10-coordinated" Fe(II) is sandwiched between two planar aromatic ligands,[1c] metal ions favoring tetrahedral or octahedral coordination have been ignored for a long time in this field because of their considerable three-dimensional

[†] Department of Inorganic, Analytical and Applied Chemistry, University of Geneva.
[‡] Laboratory of X-ray Crystallography, University of Geneva.
[§] Institut de Physique et Chimie des Matériaux de Strasbourg-IPCMS.
[⊥] Ecole Polytechnique Fédérale de Lausanne.
[∥] Department of Organic Chemistry, University of Geneva.

(1) (a) Serrano, J. L. *Metallomesogens, Synthesis, Properties and Applications*; VCH: Weinheim, Germany, 1996. (b) Donnio, B.; Guillon, D.; Deschenaux, R.; Bruce, D. W. In *Comprehensive Coordination Chemistry*; McCleverty, J. A., Meyer, T. J., Eds.; Elsevier: Oxford, U.K., 2003; Vol. 7, Chapter 79, pp 357−627. (c) Deschenaux, R.; Goodby, J. W. In *Ferrocene: Homogeneous Catalysis, Organic Synthesis, Material Sciences*; Togni, A., Hayashi, T., Eds.; VCH: Weinheim, Germany, 1995; Chapter 9, pp 471−495.
(2) Williams, D. H.; O'Brien, D. P.; Bardsley, B. *J. Am. Chem. Soc.* **2001**, *123*, 737−738.
(3) Dunitz, J. D.; Gavezzotti, A. *Acc. Chem. Res.* **1999**, *32*, 677−684.

10.1021/ja0446101 CCC: $30.25

expansions, which do not match the above-mentioned criteria. It is only during the past decade that six-coordinate Mn(I) and Re(I) centers have been successfully coordinated to rodlike bidentate carbene-imine[4] or diimine[5] ligands to produce nematic or smectic mesophases. Interestingly, columnar mesomorphism can be alternatively induced when a sufficient number (m = 12−18) of lipophilic alkyl residues are bound to the three-dimensional pseudo-octahedral core, as in [M(β-diketonate)$_3$] complexes (M = Cr, Mn, Fe).[6] This suggests that the peculiar decoration of the central core with lipophilic residues (i.e., the geometry of the interface) may overcome structural limitations evidenced by the shape of the rigid core.[7] The formation of thermotropic cubic phases with polycatenar metallomesogens is a remarkable application of this concept, and their formation can be tentatively rationalized, either by an undulation of layers originally found in smectic phases[8] or by the oscillation of columns in columnar mesophases.[9] This opens perspectives for the introduction of spherical and bulky trivalent lanthanide ions, Ln(III), into thermotropic mesophases because the latter ions prefer high coordination numbers and display no pronounced stereochemical preference.[10] A logical approach thus aims at forcing Ln(III) to enter a cavity embedded into ligands displaying rodlike or disklike anisometries.[11] For instance, Galyametdinov, Binnemans, and co-workers have intensively investigated the cylindrical [Ln(**L1**)$_3$X$_3$] complexes in which Ln(III) is coordinated by three monodentate zwitterionic Schiff bases **L1** (Chart 1) and by the three counteranions (X = nitrate, chloride, alkyl sulfate).[12] Smectogenic behavior results in agreement with the global rodlike shape of these complexes.[11,12] On the other hand, when rigid macrocyclic porphyrin or phthalocyanine platforms such as **L2** react with Ln(III) to give the neutral tabular sandwich complexes [Ln(**L2**-2H)$_2$], columnar mesomorphism is observed along the complete lanthanide series.[13] However,

Chart 1

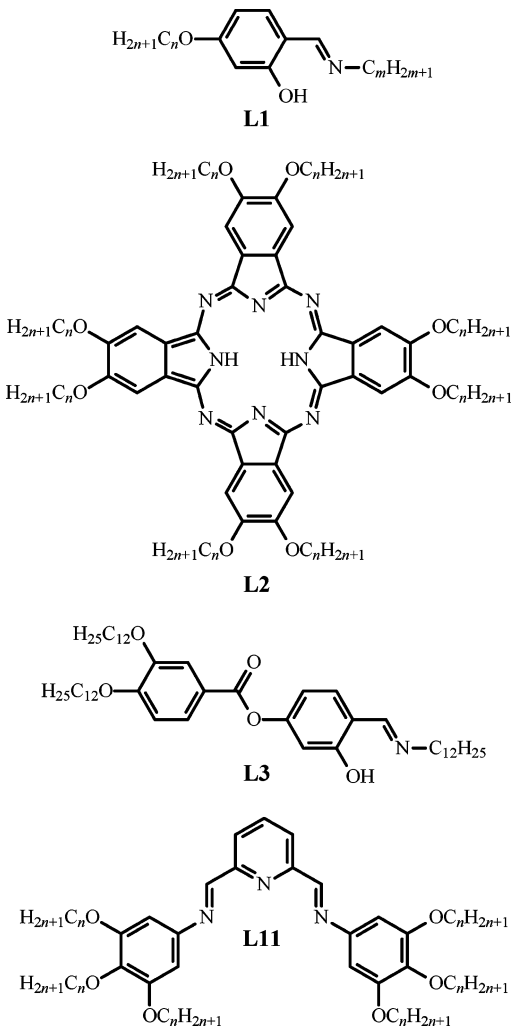

organization in mesophases is not strictly bipolarized between columnar and lamellar organization, and the same rigid core may lead to both types of mesophases assuming a judicious curvature of the interface between the incompatible parts of the molecule (alkyl chains vs rigid core). For instance, the original smectic mesophase (Sm$_A$) observed for [Ln(**L1**)$_3$X$_3$] (lamellar organization) is transformed into a columnar hexagonal arrangement (Col$_h$) in [Ln(**L3**)$_2$(**L3**-H)(CF$_3$SO$_3$)$_2$] when one additional lateral alkyl chain is connected.[14]

Inspired by these results, we have developed simple semirigid aromatic tridentate ligands, in which rodlike or bent geometries depend on the position at which the lipophilic residues are connected. Moreover, these two basic shapes interconvert upon complexation to Ln(NO$_3$)$_3$, which offers interesting perspectives for the exploration of the correlations between molecular geometries and macroscopic order (Figure 1).[15−17]

Detailed investigations of the thermal behavior of the non-coordinated trans−trans ligands **L4**−**L9** demonstrate that (1)

(4) (a) Bruce, D. W.; Liu, X. H. *Liq. Cryst.* **1995**, *18*, 165−173. (b) Liu, X.-H.; Abser, M. N.; Bruce, D. W. *J. Organomet. Chem.* **1998**, *551*, 271−280.
(5) Rowe, K. E.; Bruce, D. W. *J. Chem. Soc., Dalton Trans.* **1996**, 3913−3915.
(6) (a) Zheng, H.; Swager, T. M. *J. Am. Chem. Soc.* **1994**, *116*, 761−762. (b) Swager, T. M.; Zheng, H. *Mol Cryst. Liq. Cryst.* **1995**, *260*, 301−307.
(7) (a) Morrone, S.; Bruce, D. W.; Guillon, D. *Inorg. Chem.* **1996**, *35*, 7041−7048. (b) Ziessel, R.; Douce, L.; El-ghayoury, A.; Harriman, A.; Skoulios, A. *Angew. Chem., Int. Ed.* **2000**, *39*, 1489−1493. (c) Date, R. W.; Fernandez Iglesias, E.; Rowe, K. E.; Elliott, J. M.; Bruce, D. W. *J. Chem. Soc., Dalton Trans.* **2003**, 1914−1931.
(8) (a) Bruce, D. W. *Acc. Chem. Res.* **2000**, *33*, 831−840. (b) Diele, S. *Curr. Opin. Colloid Interface Sci.* **2002**, *7*, 333−342.
(9) (a) Donnio, B.; Heinrich, B.; Gulik-Krzywicki, T.; Delacroix, H.; Guillon, D.; Bruce, D. W. *Chem. Mater.* **1997**, *9*, 2951−2965. (b) Donnio, B.; Bruce, D. W.; Delacroix, H.; Gulik-Krzywicki, T. *Liq. Cryst.* **1997**, *23*, 147−153. (c) Donnio, B.; Rowe, K. E.; Roll, C. P.; Bruce, D. W. *Mol. Cryst. Liq. Cryst.* **1999**, *332*, 383−390.
(10) Kaltsoyannis, N.; Scott, P. *The f-Elements*; Oxford University Press: New York, 1999.
(11) For a recent comprehensive review, see: Binnemans, K.; Görller-Walrand, C. *Chem. Rev.* **2002**, *102*, 2303−2346.
(12) (a) Galyametdinov, Y.; Athanassopoulou, M. A.; Griesar, K.; Kharitonova, O.; Soto Bustamante, E. A.; Tinchurina, L.; Ovchinnikov, I.; Haase, W. *Chem. Mater.* **1996**, *8*, 922−926. (b) Binnemans, K.; Galymetdinov, Y. G.; Collinson, S. R.; Bruce, D. W. *J. Mater. Chem.* **1998**, *8*, 1551−1553. (c) Binnemans, K.; Galyametdinov, Y. G.; Van Deun, R.; Bruce, D. W.; Collinson, S. R.; Polishchuk, A. P.; Bikchantaev, I.; Haase, W.; Prosvirin, A. V.; Tinchurina, L.; Litvinov, U.; Gubajdullin, A.; Rakhmatullin, A.; Uytterhoeven, K.; Van Meervelt, L. *J. Am. Chem. Soc.* **2000**, *122*, 4335−4344. (d) van Deun, R.; Binnemans, K. *Liq. Cryst.* **2001**, *28*, 621−627. (e) Galyametdinov, Y. G.; Haase, W.; Malykhina, L.; Prosvirin, A.; Bikchantaev, I.; Rakhmatullin, A.; Binnemans, K. *Chem.−Eur. J.* **2001**, *7*, 99−105. (f) Binnemans, K.; Moors, D.; Parac-Vogt, T. N.; van Deun, R.; Hinz-Hübner, D.; Meyer, G. *Liq. Cryst.* **2002**, *29*, 1209−1216.
(13) (a) Piechocki, C.; Simon, J.; André, J. J.; Guillon, D.; Petit, P.; Skoulios, A.; Weber, P. *Chem. Phys. Lett.* **1985**, *122*, 124−128. (b) Miwa, H.; Kobayashi, N.; Ban, K.; Ohta, K. *Bull. Chem. Soc. Jpn.* **1999**, *72*, 2719−2728. (c) Binnemans, K.; Sleven, J.; De Feyter, S.; De Schryver, F. C.; Donnio, B.; Guillon, D. *Chem. Mater.* **2003**, *15*, 3930−3938.
(14) Martin, F.; Collinson, S. R.; Bruce, D. W. *Liq. Cryst.* **2000**, *27*, 859−863.
(15) Nozary, H.; Piguet, C.; Tissot, P.; Bernardinelli, G.; Bünzli, J.-C. G.; Deschenaux, R.; Guillon, D. *J. Am. Chem. Soc.* **1998**, *120*, 12274−12288.
(16) Nozary, H.; Piguet, C.; Rivera, J.-P.; Tissot, P.; Bernardinelli, G.; Vulliermet, N.; Weber, J.; Bünzli, J.-C. G. *Inorg. Chem.* **2000**, *39*, 5286−5298.
(17) Nozary, H.; Piguet, C.; Rivera, J.-P.; Tissot, P.; Morgantini, P.-Y.; Weber, J.; Bernardinelli, G.; Bünzli, J.-C. G.; Deschenaux, R.; Donnio, B.; Guillon, D. *Chem. Mater.* **2002**, *14*, 1075−1090.

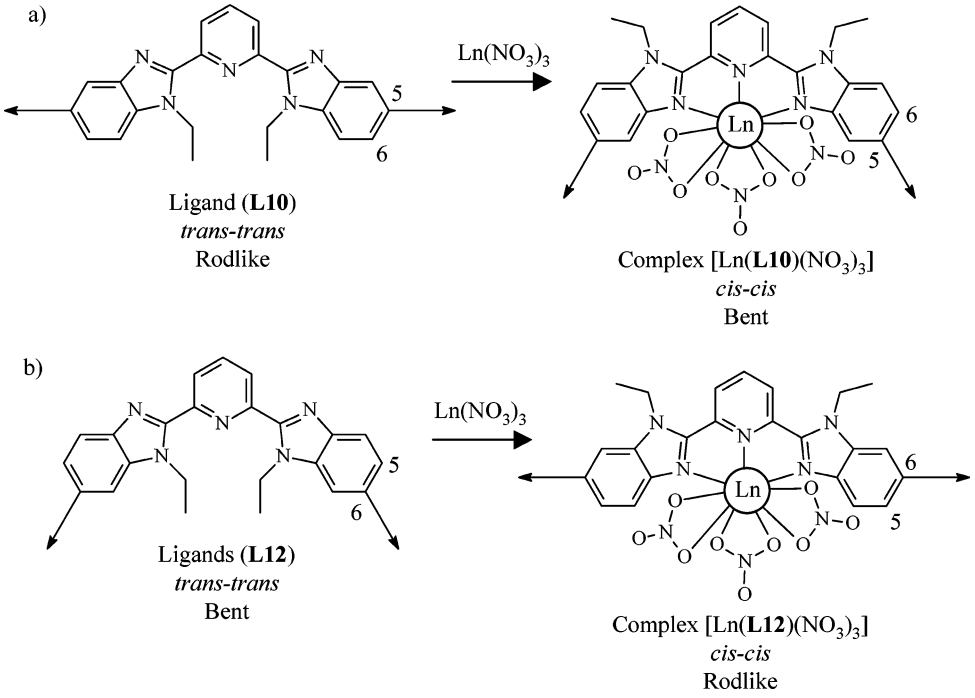

Figure 1. Conformational changes (trans−trans → cis−cis) occurring upon complexation to Ln(III) and associated molecular anisometries observed for (a) 5,5′-disubstituted ligands (**L10**) and (b) 6,6′-disubstituted ligands (**L12**).

two-atom spacers separating the tridentate binding unit from the peripheral semiflexible alkoxyaryl groups are required for inducing mesomorphism (Figure 2a),[15] (2) the nature of the two-atom spacers influences mesomorphism (Figure 2b),[15] (3) the number of intercalated 4-hydroxybenzoic groups, together with the length of the alkyl chains, affects the transition temperatures and the mesophase stabilities (Figure 2c),[15,17] and (4) the rodlike ligands provide smectic mesophases, while the bent geometry favors columnar mesomorphism (Figure 2d).[16,17]

However, the flat interfaces between the rigid core and the flexible chains in **L5**−**L9** cannot overcome the considerable perturbation of the intermolecular interactions produced by the coordination of the bulky $Ln(NO_3)_3$ units. As a consequence, no mesophase could be detected for the complexes [Ln(**L*i***)-$(NO_3)_3$] ($i = 5-9$).[15−17] The connection of four supplementary divergent dodecyloxy chains in **L10**^{C12} (Scheme 1) significantly increases the volume of the chains without affecting the volume of the rigid core. This mechanism produces a significant curvature of the interfaces in the phasmidic ligand **L10**^{C12}, which is responsible for the formation of columnar mesomorphism ($Cr \xrightarrow{25°C} Col_h \xrightarrow{61°C} I$).[18] Preliminary studies showed that the hexagonal columnar mesomorphism is maintained in the associated lutetium complex [Lu(**L10**^{C12})$(NO_3)_3$] ($Cr \xrightarrow{160°C} CoIh \xrightarrow{223°C} dec$), while the first lanthanide-containing cubic mesophase was evidenced in [Eu(**L10**^{C12})$(NO_3)_3$] ($Cr \xrightarrow{140°C} Cub \xrightarrow{\sim 200°C} dec$).[18] Although this remarkable amplification of the minor contraction of the nine-coordinate ionic radius on going from Eu(III) to Lu(III) escaped rationalization in the preliminary communication,[18] a recent report on the closely related tridentate Schiff base **L11** (Chart 1), which induces columnar mesophases (Col_r, Col_h, and Col_o) in [M(**L11**)-Cl_2] complexes (M = Mn, Co, Ni, Zn), confirms the beneficial effect provided by curved hexacatenar interfaces for the generation of mesomorphism with large metallo-organic cores.[19]

In this article, we report on (i) the characterization of the mesogenic behavior of the bent 5,5′-disubstituted hexacatenar complexes [Ln(**L10**^{C12})$(NO_3)_3$] along the complete lanthanide series (Ln = La−Lu), (ii) the comparison of this mesomorphism with that of the isomeric rodlike 6,6′-disubstituted hexacatenar complexes [Ln(**L12**^{C12})$(NO_3)_3$] (Scheme 1), and (iii) the rationalization of the molecular structural changes responsible for the switch between lamellar, columnar, and cubic mesophases. Since the exploitation of the lanthanide-centered luminescence in pure[20] or doped[21] liquid crystals is attractive for improving the brightness and angular view in liquid crystal display (LCD),[21c] the photophysical properties of the europium-containing mesophases have been investigated, particularly with the aim of probing the crystalline to liquid crystalline transitions.[22]

Results and Discussion

Syntheses of the Ligands L10^{Cn}, L12^{Cn} (n = 0, 1, 2, 3, 4, 8, 12), and Their Nitrato Complexes with Zn(II) and Ln(III). The ligands **L10**^{Cn} and **L12**^{Cn} are obtained in one step (yields = 50−70%) via the coupling of 2,6-bis(5-hydroxy-1-ethylbenzimidazol-2-yl)pyridine (**3**)[15] or 2,6-bis(6-hydroxy-1-ethylbenzimidazol-2-yl)pyridine (**4**),[16] respectively, with the adequate gallic acid derivatives **2**^{Cn}, or with benzoic acid, in the presence of 1-[3-(dimethylamino)propyl]-3ethylcarbodiimide

(18) Terazzi, E.; Bénech, J.-M.; Rivera, J.-P.; Bernardinelli, G.; Donnio, B.; Guillon, D.; Piguet, C. *J. Chem. Soc., Dalton Trans.* **2003**, 769−772.
(19) Morale, F.; Date, R. W.; Guillon, D.; Bruce, D. W.; Finn, R. L.; Wilson, C.; Blake, A. J.; Schröder, M.; Donnio, B. *Chem.−Eur. J.* **2003**, *9*, 2484−2501.
(20) (a) Binnemans, K.; Malykhina, L.; Mironov, V. S.; Haase, W.; Driesen, K.; van Deun, R.; Fluyt, L.; Görller-Walrand, C.; Galyametdinov, Y. G. *ChemPhysChem* **2001**, 680−683. (b) Binnemans, K.; Lodewyckx, K.; Parac-Vogt, T. N.; van Deun, R.; Goderis, B.; Tinant, B.; Van Hecke, K.; Van Meervelt, L. *Eur. J. Inorg. Chem.* **2003**, 3028−3033.
(21) (a) Binnemans, K.; Moors, D. *J. Mater. Chem.* **2002**, *12*, 3374−3376. (b) van Deun, R.; De Fré, B.; Moors, D.; Binnemans, K. *J. Mater. Chem.* **2003**, *13*, 1520−1522.
(22) Suarez, S.; Mamula, O.; Imbert, D.; Piguet, C.; Bünzli, J.-C. G. *Chem. Commun.* **2003**, 1226−1227.

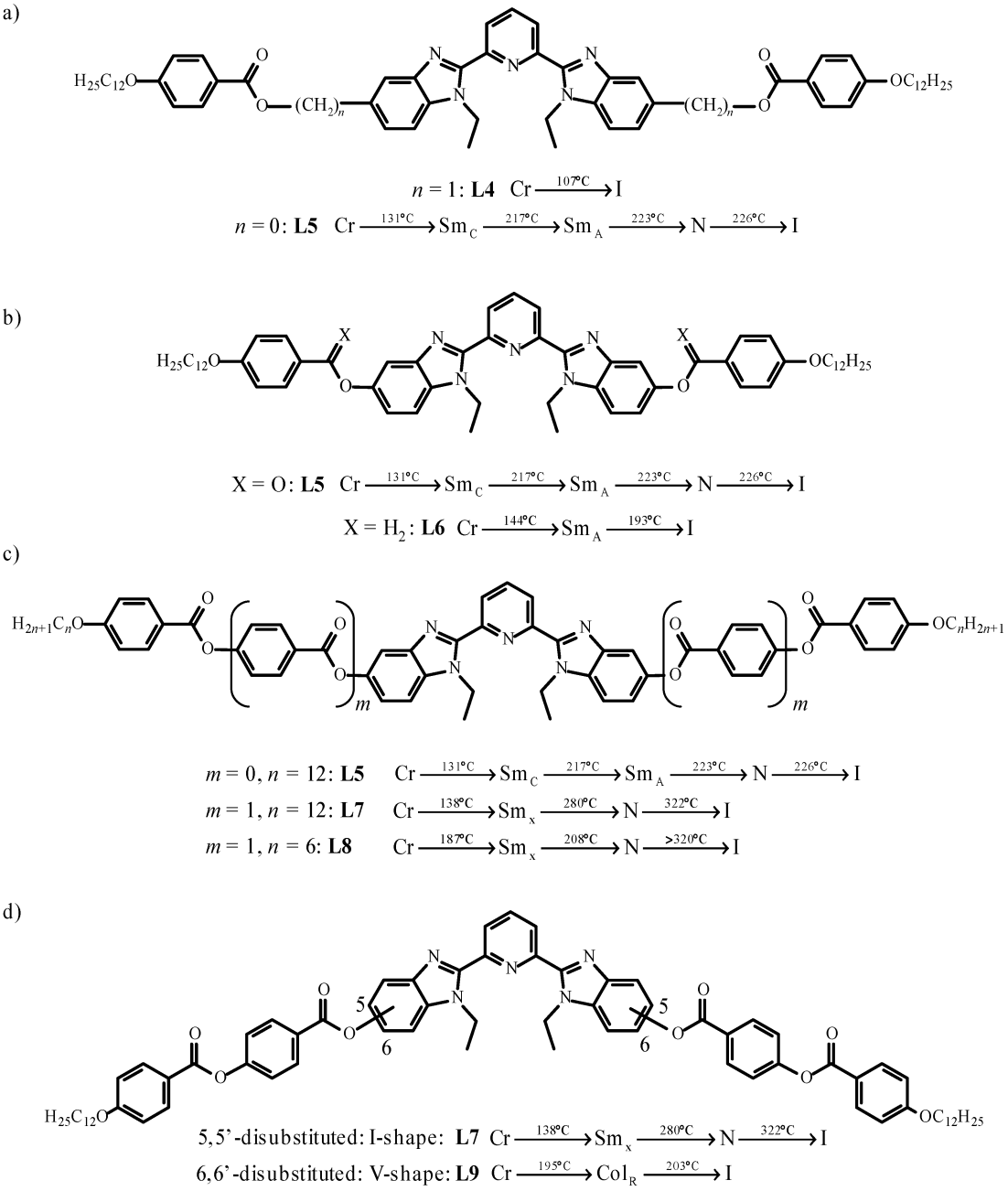

Figure 2. Mesogenic behavior of the tridentate ligands **L4**−**L9**. Illustration of the influence of (a) the length of the spacer, (b) the nature of the spacer, (c) the number of intercalated 4-hydroxy benzoic acid units and the length of the alkyl chains, and (d) the interconversion between rodlike and bent geometries (Cr: crystal, Sm_A: Smectic A, Sm_C: Smectic C, Col_r: rectangular columnar, N: nematic, I: isotropic liquid).[15−17]

(EDCI) and 4-(dimethylamino)pyridine (DMAP, Scheme 1). The ^{1}H NMR spectra confirm dynamically averaged C_{2v} symmetries on the NMR time scale for the ligands, while the lack of NOE effect between the ethyl residues and the protons connected at the meta positions of the pyridine ring agrees with the trans−trans arrangement of the 2,6-bis(benzimidazole)pyridine core previously established for **L4**−**L9**.[15−17] Reactions of $\mathbf{L10}^{Cn}$, $\mathbf{L12}^{Cn}$, with $Zn(NO_3)_2{\cdot}6H_2O$ and $Ln(NO_3)_3{\cdot}xH_2O$ (Ln = La−Lu, x = 1−4) in acetonitrile/dichloromethane produce good yields (80−90%) of the complexes $[Zn(\mathbf{L10}^{Cn})(NO_3)_2]$, $[Ln(\mathbf{L10}^{Cn})(NO_3)_3]$, and $[Ln(\mathbf{L12}^{Cn})(NO_3)_3]$ (n = 0, 1, 2, 3, 4, 8, 12; Ln = La−Lu, except Pm) containing variable amounts of cocrystallized solvent molecules (Table S1).

The 35−40 cm^{-1} blue shift observed for the C═C aromatic stretching frequency upon complexation is characteristic of meridional tricoordination of the bis(benzimidazole)pyridine units to the metal,[15−17,23] while the negligible variation of the stretching vibration of the carbonyl groups (maximum red shift ≤ 9 cm^{-1}) confirms their lack of interaction with the metal ions. Vibrational spectroscopy is also well-suited for investigating the binding mode of the nitrate anions.[24] The large separations detected between the antisymmetric (ν_a) and the symmetric (ν_s) stretching vibrations of the NO_2 group ($\Delta\nu$

(23) Petoud, S.; Bünzli, J.-C. G.; Schenk, K. J.; Piguet, C. *Inorg. Chem.* **1997**, *36*, 1345−1353.
(24) Nakamoto, K. *Infrared and Raman Spectra of Inorganic and Coordination Compounds*, 5th ed.; John Wiley & Sons: New York, 1997; Part B, pp 87−89.

Scheme 1. Synthesis and Nomenclature of the Ligands **L10**^{Cn}, **L12**^{Cn} and their Complexes [Ln(L*i*Cn)$(NO_3)_3$]

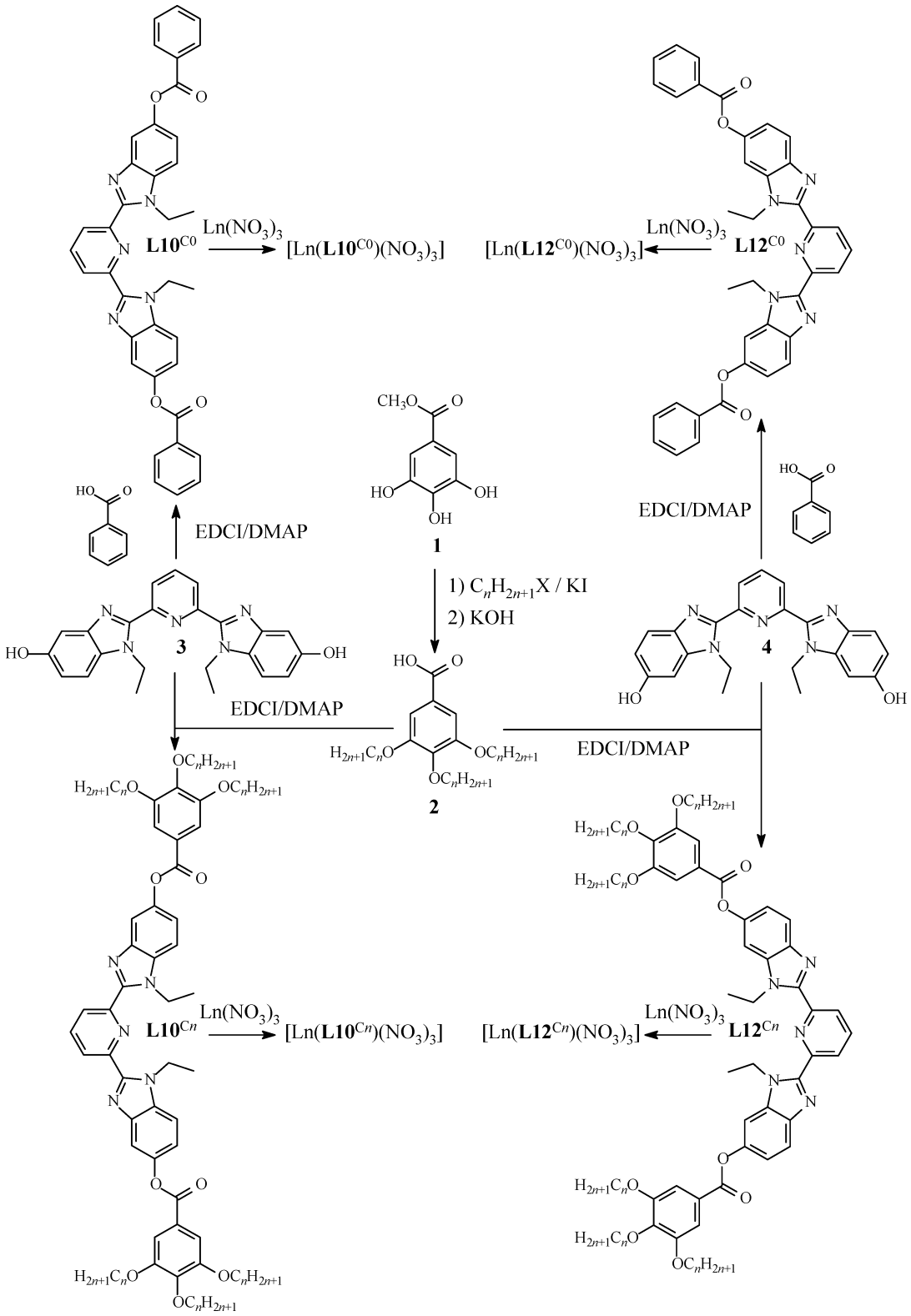

$= \nu_a - \nu_s = 178-225$ cm^{-1}, Table S2) point to bidentate coordination in all lanthanide complexes.[24] For the zinc complexes [Zn(**L10**^{Cn})$(NO_3)_2$], the large number of intense bands in the 1000−1600 cm^{-1} domain prevents a reliable assignment of $\nu(NO_2)$ stretching vibrations, and no conclusion regarding the nitrate binding mode can be drawn. Attempts to crystallize complexes with lipophilic alkoxy chains ($n = 2-12$) failed, but X-ray quality crystals could be obtained with the less lipophilic ligands having $n = 0$, 1. Diffusion of volatile ethers (i.e., diethyl-, disopropyl-, or *tert*-butylmethyl ether) into concentrated polar organic solutions of the ligand, or of the complexes, gives fragile prisms for **L10**^{C1} (**5**), [Zn(**L10**^{C1})$(NO_3)_2$]·3DMF (**6**), [La(**L10**^{C0})$(NO_3)_3(C_3H_6O)$] (**7**), [Eu(**L10**^{C0})$(NO_3)_3(CH_3CN)$]·2CH_3CN (**8**), [Yb(**L10**^{C0})$(NO_3)_3$]·CH_3CN (**9**),

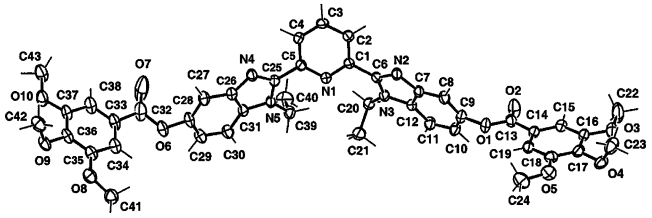

Figure 3. Perspective view of $\mathbf{L10}^{C1}$ with ellipsoids represented at the 40% probability level and numbering scheme.

$[Eu_2(\mathbf{L12}^{C0})_2(NO_3)_6]\cdot 3CH_3CN\cdot 0.5H_2O$ (**10**), and $[Lu(\mathbf{L12}^{C0})(NO_3)_3]\cdot 1.5C_3H_6O$ (**11**).

Solid-State Structures. The organization in liquid crystalline phases is reminiscent of that observed in the isotropic liquid (weak intermolecular interactions and no structural correlation) and that evidenced in the crystal (strong intermolecular interactions and long-range structural correlation). We can therefore reasonably use X-ray diffraction data collected on single crystals for modeling the molecular structure of the rigid cores in metallomesogens because their geometry and macroscopic organization are poorly affected by the melting process, mainly due to the disorganization of the terminal aliphatic chains.

Ligand $\mathbf{L10}^{C1}$ (5) and Complex $[Zn(\mathbf{L10}^{C1})(NO_3)_2]\cdot 3DMF$ (6): trans−trans versus cis−cis Conformations. In agreement with NOE measurements in solution, the aromatic 2,6-bis(benzimidazol-2-yl)pyridine unit of the noncoordinated ligand $\mathbf{L10}^{C1}$ adopts the usual trans−trans conformation in the solid state (i.e., both N2 and N4 atoms adopt a trans conformation relative to N1, Figure 3). This conformation provides an approximate rodlike arrangement of the rigid core, and the considerable interplanar angles between the gallic ester and the benzimidazole ring to which it is connected (63.9° and 68.0°, Table S3) eventually induce a crosshatched organization of the successive aromatic units in $\mathbf{L10}^{C1}$, as previously reported for **L8** (Figure 3).[17]

The ligand $\mathbf{L10}^{C1}$ is thus considered as a central "planar" tridentate aromatic core (pyridine−benzimidazole interplanar angles: 30.4° and 39.4°, Table S3), flanked with two appended "perpendicular" gallic ester groups. Comparison with the crystal structure of the higher homologue $\mathbf{L10}^{C4}$ shows only minor structural variations between the tridentate units (Figure S1),[18] which implies that the length of the flexible alkyl chains has no significant effect on the rigid core. This crosshatched arrangement provides two privileged pseudo-orthogonal directions, along which intermolecular π-staking between the rigid cores may develop in the crystal. Three such interactions are indeed detected in $\mathbf{L10}^{C1}$; two involve molecules related by inversion centers (gallic ester/gallic ester, $d = 3.67$ Å, and benzimidazole/benzimidazole, $d = 3.56$ Å), while the third one occurs between one benzimidazole ring and one gallic ester residue belonging to two different molecules related by a mirror plane ($d = 3.34$ Å, Figure S2).

Upon complexation to $Zn(NO_3)_2$ in **6**, the three nitrogen atoms N1, N2, and N4 of the almost planar tridentate ligand adopt a cis−cis conformation (pyridine−benzimidazole interplanar angles = 10.1−12.0°, Table S4). In this case, the connection of the gallic acid residues at the 5,5′-positions produces an approximate bent geometry for the coordinated ligand. One oxygen atom of each monodentate nitrate anion completes a distorted trigonal bipyramidal (tbp) environment around Zn(II), in which the two N(bzim) (N2, N4) occupy the apical positions (Figure 4, Table S5), as previously reported for $[Zn(\mathbf{L11})Cl_2]$[19] and $[Zn(\mathbf{L13})(NO_3)_2]$ (Figure S3).[18]

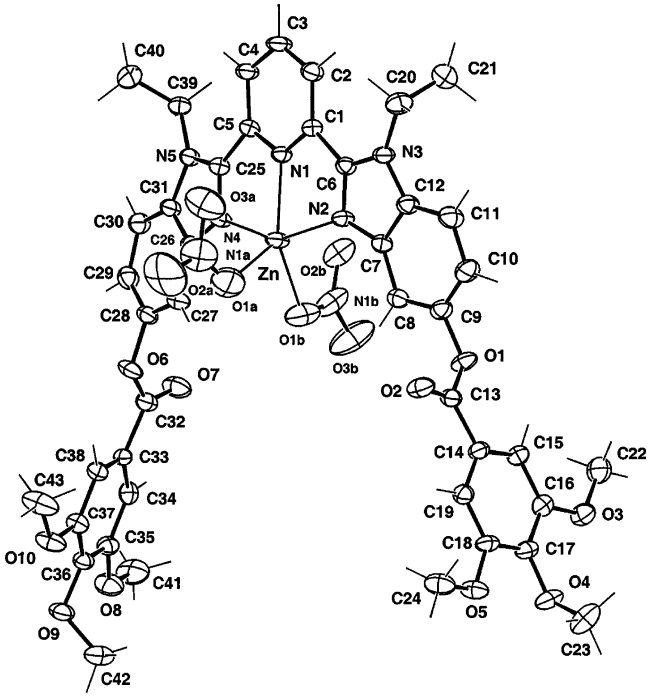

Figure 4. Perspective view of $[Zn(\mathbf{L10}^{C1})(NO_3)_2]$ in the crystal of **6** with ellipsoids represented at the 40% probability level and numbering scheme. The nonbonded DMF molecules have been omitted for clarity.

Again, the gallic esters in **6** show large interplanar angles with the benzimidazole rings to which they are connected (56.1° and 89.6°, Table S4), thus favoring two pseudo-orthogonal directions for intermolecular π-stacking interactions, which are observed in the crystal. (Figure S4).

We conclude that the free $\mathbf{L10}^{Cn}$ ligands adopt the trans−trans conformation leading to rodlike anisometry (Figure 3), while their tricoordination to a metal ion produces the expected conformational change providing a bent arrangement in the complexes (Figure 4). Moreover, the crosshatched organization of the aromatic sidearms is not affected by the complexation process. The latter structural feature allows weak intermolecular interactions to develop along two privileged pseudo-orthogonal directions in the crystals.

Bent Complexes with $\mathbf{L10}^{C0}$ (7−9). Crystals **7**−**9** contain neutral monometallic complexes $[La(\mathbf{L10}^{C0})(NO_3)_3(C_3H_6O)]$, $[Eu(\mathbf{L10}^{C0})(NO_3)_3(CH_3CN)]$, and $[Yb(\mathbf{L10}^{C0})(NO_3)_3]$, together with interstitial solvent molecules. Complexes **7** and **8** can be considered as being isostructural, while **9** possesses a different structure. The cis−cis conformation of the roughly planar tricoordinated aromatic ligand $\mathbf{L10}^{C0}$ (pyridine−benzimidazole interplanar angles: 5.7−30.4°, average 13(9)°, Tables S6−S8) is similar to that found in the zinc complex **6**, while the geometry and coordination of the three bound bidentate nitrate anions are comparable in the three complexes **7**−**9** (Figure 5).

The contraction of the lanthanide ionic radii, in going from La to Yb, is responsible for the removal of the extra solvent molecule bound in the first coordination sphere of the large 10-coordinate ions in **7** (La) and **8** (Eu), leading to a nine-coordinate ion in **9** (Yb, Figure 5), but the common LnN_3O_6 cores are almost superimposable (Figure S5). This behavior parallels a similar decrease in the coordination number when

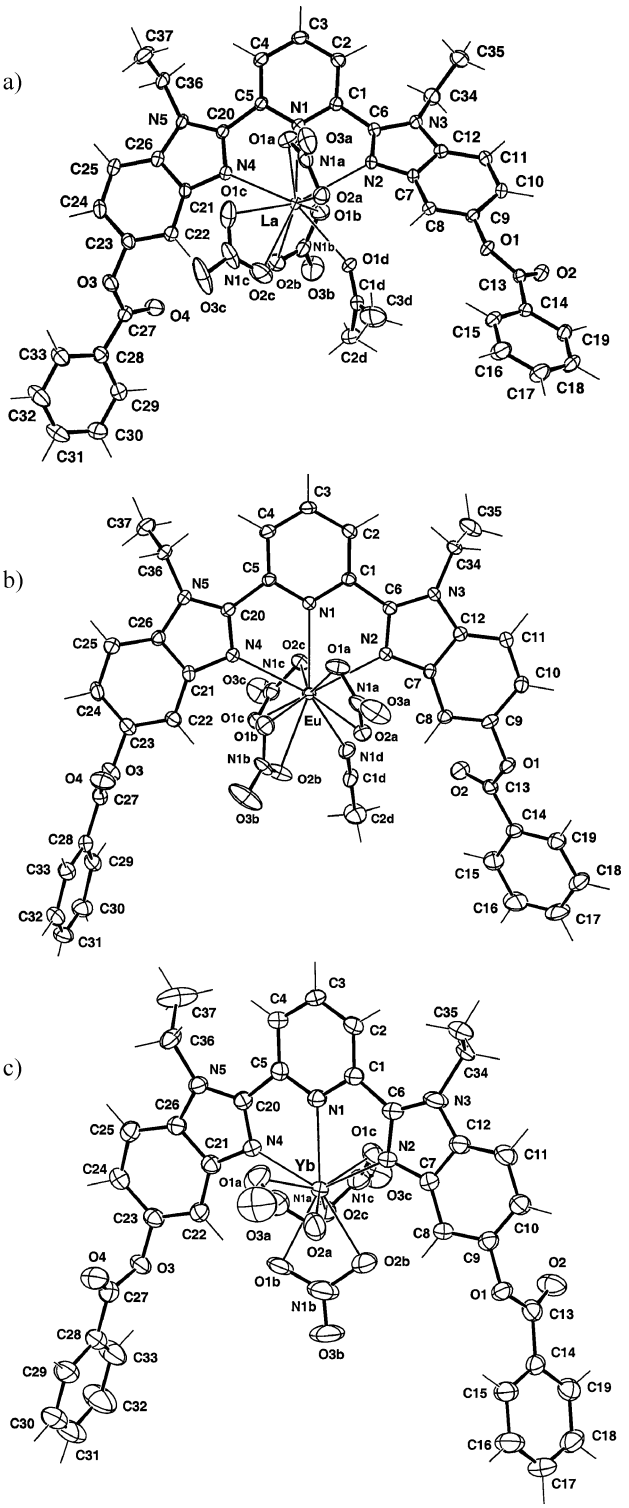

Figure 5. Perspective views of (a) [La(**L10**^{C0})$(NO_3)_3(C_3H_6O)$] in the crystal of **7**, (b) [Eu(**L10**^{C0})$(NO_3)_3(CH_3CN)$] in the crystal of **8**, and (c) [Yb(**L10**^{C0})$(NO_3)_3$] in the crystal of **9** with ellipsoids represented at the 40% probability level and numbering schemes. The nonbonded solvent molecules have been omitted for clarity.

going from [Eu(**L13**)$(NO_3)_3(CH_3OH)$] (10-coordinated)[25] to [Lu(**L15**)$(NO_3)_3$] (nine-coordinated).[15] The lack of strong steric constraints in complexes **7**−**9** is testified by standard Ln−O and Ln−N bond distances (Table S9), which allows the calculation of standard experimental ionic radii $R_{La}^{CN=10}$ = 1.264 Å (expected 1.27 Å),[26] $R_{Eu}^{CN=10}$ = 1.142 Å (expected 1.17 Å),[25] and $R_{Yb}^{CN=9}$ = 1.046 Å (expected 1.042 Å),[26] by using Shannon's definition with r(N) = 1.46 Å[26] and r(O) = 1.31 Å.[27] As previously noticed for [Zn(**L10**^{C1})$(NO_3)_2$] (**6**), the gallic esters in **7**−**9** display significant torsions with respect to the benzimidazole rings to which they are connected (18.5−83.3°, average 55(23)°, Tables S6−S8). This mechanism provides the usual crosshatched arrangement of the semirigid aromatic units along the bent strand coordinated to Ln$(NO_3)_3$ (Figure 5). As a consequence, gallic ester/gallic ester and benzimidazole/benzimidazole π-stacking interactions systematically occur in the crystals of **7**−**9** (Figures S6−S8).

Rodlike Complexes with L12^{C0} **(10−11).** As previously established for the complexes with **L10**^{C0}, the decrease of the coordination number from CN = 10 in [Eu_2(**L12**^{C0})$_2(NO_3)_6$] (**10**) to CN = 9 in [Lu(**L12**^{C0})$(NO_3)_3$] (**11**) is ascribed to the contraction of the lanthanide radii (Figure 6). The tricoordinated 6,6′-disubstituted rodlike ligand **L12**^{C0} in **10** and **11** adopts the expected cis−cis conformation, which is compatible with a close approach of two monometallic building blocks in the crystal structures. In **10**, the trend of Eu(III) to reach 10-coordinate environments allows the formation of two intermetallic oxygen bridges involving two oxygen atoms of the equatorial nitrate anions (O1c and O1d, Figure 6a). The resulting Eu−$O_{bridging}$ bond distances (2.51−2.63 Å, average 2.57(6) Å, Table S10) are marginally longer than the Eu−$O_{nonbridging}$ bonds (2.44−2.60 Å, average 2.50(6) Å, Table S10), and **10** can be best described as a neutral pseudo-centrosymmetric bimetallic complex [Eu_2(**L12**^{C0})$_2(NO_3)_6$] with a relatively short intermetallic distance Eu···Eu = 4.5186(10) Å.

The Eu−N bonds in the bimetallic complex [Eu_2(**L12**^{C0})$_2$-$(NO_3)_6$] (average Eu−N_{py} = 2.63(1) Å, average Eu−$N_{benzimid}$ = 2.54(2) Å, Table S10) are comparable with those found in the bent monometallic analogue [Eu(**L10**^{C0})$(NO_3)_3(CH_3CN)$] (**8**: Eu−N_{py} = 2.617(2) Å, average Eu−$N_{benzimid}$ = 2.51(2) Å, Table S9), which points to negligible interstrand repulsions in the dimer, as further supported by the calculated 10-coordinate ionic radii in **10** ($R_{Eu}^{CN=10}$ = 1.18 Å, expected 1.17 Å).[25,26] As usual, the tridentate bis(benzimidazole)pyridine units are roughly planar (interplanar angles 15.3−27.5°), while the terminal gallic esters exhibit significant torsions (16.7−87.8°, average 61(31)°, Table S11). Interestingly, the dimeric complex displays no significant intermolecular interaction because the gallic esters and the benzimidazole rings are less accessible in these rodlike molecules (Figure S9).

In the related monometallic Lu complex **11**, the smaller Lu(III) ion is nine-coordinated, and no Lu−$O_{bridging}$ bond is detected (Figure 6b). However, two slightly different complexes are observed in the asymmetric unit that adopt a quasi-centrosymmetric arrangement reminiscent of that found in [Eu_2(**L12**^{C0})$_2(NO_3)_6$]. The nonbonded Lu···Lu distance in **11** (6.6446(4) Å) is obviously longer than the related intramolecular intermetallic separation in the Eu dimer, but it is short enough to confirm that the coordinated rodlike ligands are compatible with a close approach of the monometallic building blocks. The lack of propensity of Lu(III) to expand its coordination number

(25) Piguet, C.; Williams, A. F.; Bernardinelli, G.; Moret, E.; Bünzli, J.-C. G. *Helv. Chim. Acta* **1992**, *75*, 1697−1717.
(26) Shannon, R. D. *Acta Crystallogr.* **1976**, *A32*, 751−767.
(27) Bünzli, J.-C. G.; Klein, B.; Chapuis, G.; Schenk, K. J. *Inorg. Chem.* **1982**, *21*, 808−812.

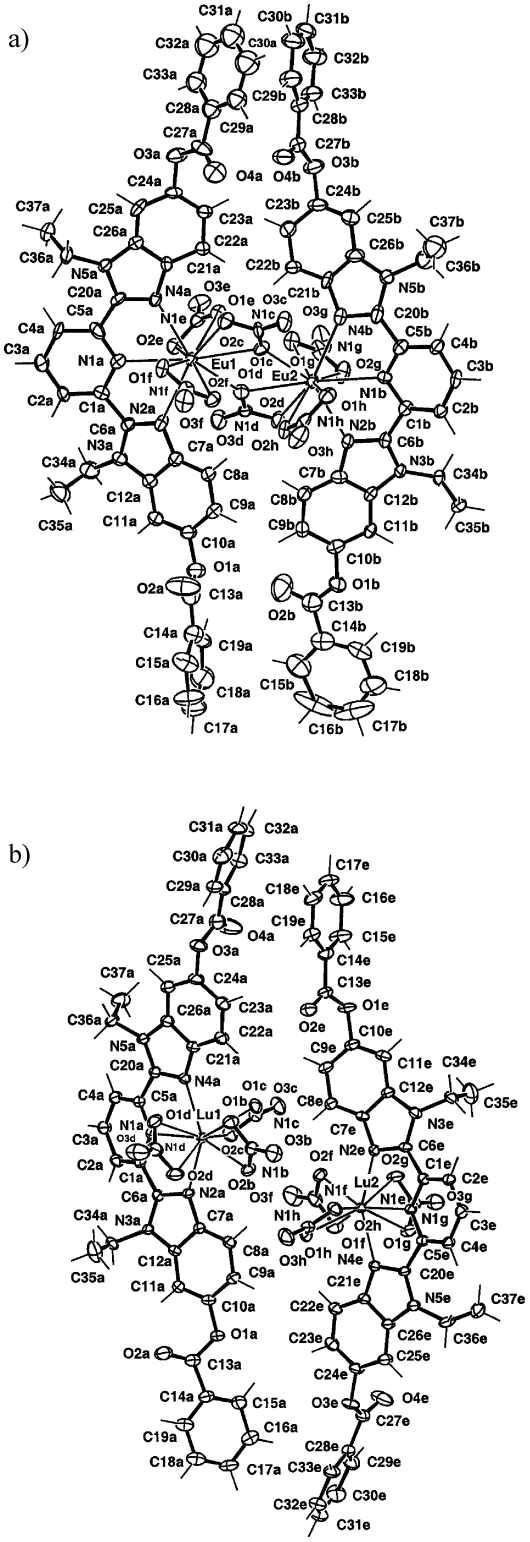

Figure 6. Perspective views of (a) $[Eu_2(\mathbf{L12}^{C0})_2(NO_3)_6]$ in the crystal of **10** and (b) $[Lu(\mathbf{L12}^{C0})(NO_3)_3]$ in the asymmetric unit of the crystal of **11** with numbering scheme. Ellipsoids are represented at the 40% probability, and the nonbonded solvent molecules have been omitted for clarity.

explains its reluctance to form the bridged dimer. The calculated ionic radii $R_{Lu}^{CN=9} = 1.032$ Å exactly match that expected for nine-coordinate Lu(III),[26] in agreement with standard Lu−O and Lu−N bond lengths (Table S10). Again, the ligand adopts the usual crosshatched configuration with a roughly planar tridentate binding unit (interplanar angles 19.4−20.3°), and terminal gallic esters displaying significant torsions (54.4−78.4°, Table S12). Since the central aromatic core is less embedded in $[Lu(\mathbf{L12}^{C0})(NO_3)_3]$ (Figure 6b) than in $[Eu_2(\mathbf{L12}^{C0})_2(NO_3)_6]$ (Figure 6a), the pyridine−benzimidazole units of neighboring complexes related by inversion centers are involved in head-to-tail π-stacking intermolecular interactions ($d_{py-benzimid} = 3.11-3.72$ Å, Figure S10).

From this study, we conclude that (1) the tricoordinated cis−cis ligand strands $\mathbf{L10}^{C0}$ and $\mathbf{L12}^{C0}$ control the global anisometry of the complexes by adopting respectively bent and rodlike crosshatched arrangements, (2) the smaller lanthanides (Yb, Lu) display nine-coordination with three bidentate nitrate anions completing the coordination sphere, while the larger lanthanides (La, Eu) expand their coordination number to 10 via either fixation of an extra solvent molecule (bent complexes) or dimerization of two monometallic building blocks sharing two nitrate anions (rodlike complexes), and (3) efficient intermolecular π-stacking interactions in monometallic complexes occur along two pseudo-orthogonal directions defined by the orientation of the coordinated tridentate binding unit and one of the gallic esters. These points are crucial for further interpretation of the intermolecular interactions occurring between rigid cores in the liquid crystalline state (vide infra).

Solution Structure of the Nitrato Complexes $[Ln(\mathbf{L12}^{C0})(NO_3)_3]$, $[Ln(\mathbf{L12}^{C12})(NO_3)_3]$, and $[Ln(\mathbf{L10}^{C12})(NO_3)_3]$ (Ln = La, Eu, Lu). Since intermolecular interactions are weaker in liquid crystals than in crystals, some flexibility, reminiscent of molecules in solution, must be combined with solid-state structural models for providing a reliable picture of the molecular and macroscopic organizations evidenced in mesophases. ^{1}H NMR spectroscopy is particularly efficient for addressing solution structures of lanthanide complexes.[28] The ^{1}H NMR spectrum of the nonlipophilic diamagnetic complex $[Lu(\mathbf{L12}^{C0})(NO_3)_3]$ in $CD_3CN/(CD_3)_2CO$ (4:1) shows the 10 signals expected for an average C_{2v} symmetry on the NMR time scale (Figure S11a), obtained by a minor relaxation of the monometallic molecular structure evidenced for **11** in the solid state (Figure 6b). The significant downfield complexation shift observed for H1 upon coordination to Lu(III) ($\Delta\delta = 0.73$ ppm, Table 1) is diagnostic for the coordination of the central pyridine ring,[15−17,29] while the detection of NOE effects between H9···H2 and H10···H2 confirms the cis−cis conformation of the tridentate binding unit resulting from the concomitant coordination of the benzimidazole sidearms. In conclusion, the meridional tricoordination of $\mathbf{L12}^{C0}$ to Lu(III) established in the solid state (Figure 6b) is maintained in solution.

Although we expect no signal in mass spectrometry for neutral complexes, some residual ESI-MS peaks are detected when a solution of the Lu complex **11** in acetonitrile/acetone is sprayed. The most intense peak occurring at $m/z = 964.0$ can be assigned to $[Lu(\mathbf{L12}^{C0})(NO_3)_2(C_3H_6O)]^+$ in which one nitrate has been replaced by an acetone molecule. The minor peaks observed at $m/z = 1513.1$ ($[Lu(\mathbf{L12}^{C0})_2(NO_3)_2]^+$) and $m/z =$

(28) (a) Peters, J. A.; Huskens, J.; Raber, D. J. *Prog. Nucl. Magn. Reson. Spectrosc.* **1996**, *28*, 283−350. (b) Forsberg, J. H. In *Handbook on the Physics and Chemistry of Rare Earths*; Gschneidner, K. A., Jr., Eyring, L., Eds.; Elsevier: Amsterdam, 1996; Vol. 23, Chapter 153, pp 1−68. (c) Piguet, C.; Geraldes, C. F. G. C. In *Handbook on the Physics and Chemistry of Rare Earths*; Gschneidner, K. A., Jr., Bünzli, J.-C. G., Pecharsky, V. K., Eds.; Elsevier Science: Amsterdam, 2003; Vol. 33, pp 353−463.
(29) Lavallee, D. K.; Baughman, M. D.; Phillips, M. P. *J. Am. Chem. Soc.* **1977**, *99*, 718−724.

Table 1. ^{1}H NMR Chemical Shifts for $\mathbf{L12}^{C0}$ and [Ln($\mathbf{L12}^{C0}$)$(NO_3)_3$] in $CD_3CN/(CD_3)_2CO$ (4:1)·(Numbering Scheme in Figure S11)

	H1	H2	H3	H4	H5	H6	H7	H8	H9	H10
$\mathbf{L12}^{C0}$	8.05	8.33	7.35	7.17	7.87	8.22	7.49	7.61	4.76	1.34
[La($\mathbf{L12}^{C0}$)$(NO_3)_3$]	8.60	8.37	7.60	6.92	7.34	8.40−8.80	7.50−7.80	7.5−7.8	4.70	1.72
[Eu($\mathbf{L12}^{C0}$)$(NO_3)_3$]	7.11	6.41	8.07	9.43	16.56	8.76	7.87−7.97	7.87−7.97	5.82	2.21
[Lu($\mathbf{L12}^{C0}$)$(NO_3)_3$]	8.78	8.76	7.93	7.53	8.29	8.24	7.65	7.78	5.05	1.80

1874.0 ($[Lu_2(\mathbf{L12}^{C0})_2(NO_3)_5]^+$) suggest that a dimerization process, leading to $[Lu_2(\mathbf{L12}^{C0})_2(NO_3)_6]$, occurs in solution. However, the exclusive detection of the monometallic C_{2v} symmetrical complex by ^{1}H NMR (Figure S11a) indicates that such an equilibrium can be neglected for Lu, within the limit of sensitivity of this technique (≥2%). This approximation does not hold for the corresponding La and Eu complexes which generate two series of ^{1}H NMR signals (Figures S11b,c). In the latter cases, the residual ESI-MS signals show strong peaks arising from the bimetallic dimers $[Ln_2(\mathbf{L12}^{C0})_2(NO_3)_5]^+$ (Eu: $m/z = 1828.1$; La: $m/z = 1802.2$), while only faint peaks can be assigned to the monometallic complexes $[Ln(\mathbf{L12}^{C0})(NO_3)_2(C_3H_6O)]^+$ (Eu: $m/z = 942.6$; La: $m/z = 928.1$). A combination of these observations with the dual isolation of the monometallic complex **11** for Lu (Figure 6b) and the bimetallic bridged dimer **10** for Eu (Figure 6a) suggests that the dimerization process (eq 1) becomes sizable for large Ln(III) ions, that is, the associated thermodynamic constants $K_d^{Ln-L12^{C0}}$ decrease in going from La to Lu.

$$2[Ln(\mathbf{Li}^{Cn})(NO_3)_3] \rightleftharpoons [Ln_2(\mathbf{Li}^{Cn})_2(NO_3)_6]\ K_d^{Ln-Li^{Cn}} \quad (1)$$

This mechanism is further supported by NMR diffusion measurements[30] performed on the analogous lipophilic complexes [Ln($\mathbf{L12}^{C12}$)$(NO_3)_3$] in CD_2Cl_2. Their ^{1}H NMR spectra closely resemble those recorded for [Ln($\mathbf{L12}^{C0}$)$(NO_3)_3$], which implies the existence of a single C_{2v} symmetrical complex for Lu, while mixtures of two complexes in variable ratios are detected for La and Eu (Figure S12). Assuming that (i) the Einstein−Smoluchowski−Stokes auto-diffusion theory holds for our lipophilic complexes and (ii) the molecules in solution can be roughly modeled by spheres possessing an hydrodynamic radius r_h, the auto-diffusion coefficient D_m at a fixed temperature in CD_2Cl_2 is proportional to $(\bar{\nu}_m \cdot MM_m)^{-1/3}$, where MM_m stands for the molecular mass of the molecule and $\bar{\nu}_m$ stands for its specific partial volume.[30] The determination of D_m by diffusional NMR for shape-similar complexes and/or ligands is thus an efficient tool for deducing the molecular mass of an unknown species (x) in solution, when a reference compound (r) is measured under the same conditions (eq 2).[31]

$$\frac{D_x}{D_r} = \sqrt[3]{\frac{\bar{\nu}_r \cdot MM_r}{\bar{\nu}_x \cdot MM_x}} \quad (2)$$

For the rodlike complex [Lu($\mathbf{L12}^{C12}$)$(NO_3)_3$], which exists as a single species in CD_2Cl_2, NMR-DOSY experiments give $D_{Lu-L12^{C12}} = 5.5(1) \times 10^{-10}$ m^2·s^{-1}, which can be compared with $D_{L12^{C12}} = 6.5(1) \times 10^{-10}$ m^2·s^{-1} measured for the free ligand $\mathbf{L12}^{C12}$ ($MM_{L12^{C12}} = 1713$ g/mol). Application of eq 2 with $\bar{\nu}_{L12^{C12}} \approx \bar{\nu}_{Lu-L12^{C12}}$ leads to $MM_{LuL12^{C12}} \approx 2800(300)$ g/mol, which compares reasonably well with 2073 g/mol calculated for the monometallic nitrato complex. We cannot expect a much better agreement because the hypothesis that both the flexible ligand and the semirigid complex behave as spheres in solution is too approximate. Recently, a detailed investigation of the formation of almost identical diastereoselective ion pairs in organic solution showed that their diffusion coefficients differ by 6%.[32] A parallel spectrophotometric titration of $\mathbf{L10}^{C12}$ with $Lu(NO_3)_3 \cdot 3H_2O$ in CH_2Cl_2/CH_3CN (1:1) shows a single end point for the ratio $\mathbf{L10}^{C12}$/Ln = 1.0 (Figure S13). The experimental data can be satisfyingly fitted with nonlinear least-squares techniques[33] to equilibrium 3 ($\log(\beta_{11}^{Lu}) = 6.1(2)$), which confirms that (i) no significant (<1%) decomplexation occurs for the complexes at millimolar concentration, and (ii) dimerization is negligible for Ln = Lu.

$$\mathbf{L10}^{C12} + Ln(NO_3)_3 \rightleftharpoons [Ln(\mathbf{L10}^{C12})(NO_3)_3]\ \beta_{11}^{Ln} \quad (3)$$

These data, combined with the low molecular mass found above for the Lu complex, indicate that [Lu($\mathbf{L12}^{C12}$)$(NO_3)_3$] exists in solution as a neutral monometallic complex with an idealized C_{2v} symmetry, reminiscent of that found in the solid state (Figure 6b). Further DOSY experiments performed on [Eu($\mathbf{L12}^{C12}$)$(NO_3)_3$] in CD_2Cl_2 demonstrate that the first series of peaks (series A in Figure S14) corresponds to a single species with $D_A = 5.7(4) \times 10^{-10}$ m^2·s^{-1}, while the second series (B) is assigned to a different species that diffuses slightly slower: $D_B = 4.6(2) \times 10^{-10}$ m^2·s^{-1}. The ratio $D_A/D_B = 1.24(2)$ translates into $MM_B/MM_A = 1.9(1)$ (eq 2), which confirms that B is a dimer. Finally, the diffusion coefficient obtained for complex A ($D_A = 5.7(4) \times 10^{-10}$ m^2·s^{-1}) matches that previously found for the monometallic complex [Lu($\mathbf{L12}^{C12}$)$(NO_3)_3$] ($D_{Lu-L12^{C12}} = 5.5(1) \times 10^{-10}$ m^2·s^{-1}). We conclude that the Eu complex exists in solution as a mixture of the monometallic unit [Eu($\mathbf{L12}^{C12}$)$(NO_3)_3$] (species A) and the bimetallic dimer [$Eu_2(\mathbf{L12}^{C12})_2(NO_3)_6$] (species B).

Variable-temperature NMR data in CD_2Cl_2 (273−313K) show that the [Eu($\mathbf{L12}^{C12}$)$(NO_3)_3$]/[$Eu_2(\mathbf{L12}^{C12})_2(NO_3)_6$] ratio smoothly increases from 1.12 (273 K) to 2.88 (313 K, Figure S15a). Calculation of $K_d^{Eu-L12^{C12}}$ (equilibrium 1) for each temperature, followed by application of van't Hoff equation (eq 4) allows the estimation of $\Delta H_d^{Eu-\mathbf{L12}^{C12}} = -25(2)$ kJ·mol^{-1} and $\Delta S_d^{Eu-\mathbf{L12}^{C12}} = -47(5)$ J·mol^{-1}·K^{-1} (Figure S15b).

$$-R \ln(K_d^{Eu-Li^{C12}}) = \frac{\Delta H_d^{Eu-Li^{C12}}}{T} - \Delta S_d^{Eu-Li^{C12}} \quad (4)$$

(30) (a) Stilbs, P. *Prog. Nucl. Magn. Reson. Spectrosc.* **1986**, *19*, 1−45. (b) Waldeck, A. R.; Kuchel, P. W.; Lennon, A. J.; Chapman, B. E. *Prog. Nucl. Magn. Reson. Spectrosc.* **1997**, *30*, 39−68. (c) Pregosin, P. S.; Martinez-Viviente, E.; Anil Kumar, P. G. *J. Chem. Soc., Dalton Trans.* **2003**, 4007−4014.
(31) Greenwald, M.; Wessely, D.; Goldberg, I.; Cohen, Y. *New J. Chem.* **1999**, 337−344.
(32) Martinez-Viviente, E.; Pregosin, P. S.; Vial, L.; Herse, C.; Lacour, J. *Chem.−Eur. J.* **2004**, *10*, 2912−2918.
(33) (a) Gampp, H.; Maeder, M.; Meyer, C. J.; Zuberbühler, A. *Talanta* **1985**, *32*, 1133−1139. (b) Gampp, H.; Maeder, M.; Meyer, C. J.; Zuberbühler, A. *Talanta* **1986**, *33*, 943−951.

These parameters are typical for a dimerization process occurring in a noncoordinating solvent for Ln(III), such as CD_2Cl_2, because the formation of the dimer is enthalpically driven (formation of two additional Eu−O bonds without breaking Eu-solvent bonds), but entropically limited (decrease of the translational entropy when two monomers dimerize). The formation of the dimer in CD_2Cl_2 is thus favored (i) at low-temperature and (ii) for 10-coordinate lanthanides as found in $[Eu_2(\mathbf{L12}^{C12})_2(NO_3)_6]$ and $[La_2(\mathbf{L12}^{C12})_2(NO_3)_6]$ (Figure S12). However, this trend is reversed in coordinating solvent because (i) the competition for the 10-coordinated site strongly reduces the enthalpic contribution and (ii) the release of two solvent molecules upon dimerization inverts the entropic trend. The latter points explain the difficulty in crystallizing the dimer out of acetonitrile solutions at room temperature, even for large Ln(III) ions.

The related isomeric bent complexes $[Ln(\mathbf{L10}^{C12})(NO_3)_3]$ (Ln = La, Eu, Lu) display ^{1}H NMR spectra strictly analogous to those discussed above for $[Ln(\mathbf{L12}^{C12})(NO_3)_3]$, with the exclusive formation of the monometallic complex $[Lu(\mathbf{L10}^{C12})(NO_3)_3]$ in CD_2Cl_2, while a mixture of monometallic and bimetallic dimeric complexes are observed with the larger lanthanides (Ln = La, Eu). NMR DOSY experiments performed on the $[Eu(\mathbf{L10}^{C12})(NO_3)_3]/[Eu_2(\mathbf{L10}^{C12})_2(NO_3)_6]$ mixture indicate the existence of only two complexes in solution with $D_A = 4.5(1) \times 10^{-10}$ m^2·s^{-1} and $D_B = 3.5(4) \times 10^{-10}$ m^2·s^{-1} (Figure S16a). The ratio $D_A/D_B = 1.29(2)$ translates into $MM_B/MM_A = 2.1(1)$ (eq 2), which confirms the dimer/monomer relationship between these complexes. Application of the van't Hoff eq 4 to the VT-NMR data recorded in CD_2Cl_2 gives $\Delta H_d^{Eu-L10^{C12}} = -54(4)$ kJ·mol^{-1} and $\Delta S_d^{Eu-L10^{C12}} = -162(16)$ J·mol^{-1}·K^{-1} (equilibrium 1), which points to a sizable enthalpic driving force for the formation of the dimer (Figure S16b). From this set of NMR data, we conclude that the bent ($i = 10$) or rodlike ($i = 12$) monometallic molecular structures found for the complexes $[Ln(\mathbf{L}\textit{i}^{C0})(NO_3)_3]$ in the solid state (Ln = La, Eu, Yb, Lu) are maintained in solution along the complete lanthanide series. However, dimeric bimetallic complexes similar to the one evidenced in the crystal structure of $[Eu_2(\mathbf{L12}^{C0})_2(NO_3)_6]$ systematically coexist in solution with the monometallic building block (eq 1). For large Ln(III), the dimer becomes the major product in noncoordinating solvents at low temperature.

Organization of the ligands L10^{C12} and L12^{C12} and of their Nitrato Lanthanide Complexes in the Liquid Crystalline State. The connection of six lipophilic alkoxy chains to the tridentate rigid cores in $\mathbf{L10}^{C12}$ and $\mathbf{L12}^{C12}$ favors a thermally driven microsegregation process resulting from the huge entropic release accompanying the melting of the flexible chains.[2] The detailed investigation of $\mathbf{L10}^{Cn}$ ($n = 1, 2, 3, 4, 8, 12$) shows that $n = 12$ corresponds to the minimum length for which a well-defined two-step melting process is observed Cr $\xrightarrow{25°C}$ Col_h $\xrightarrow{61°C}$ I (Table 2).

Polarized light microscopy (PLM) of the $\mathbf{L10}^{C12}$ mesophase displays a fan texture with cylindrical domains and with a homeotropic zone, which altogether are typical of a hexagonal columnar mesophase (Col_h, Figure S17). The transition from the crystal into the columnar mesophase (Cr → Col_h) cannot be reliably detected by differential scanning calorimetry (DSC) (i.e., a weak drift of the baseline is detected), but small-angle X-ray diffraction profiles (SA-XRD) unambiguously show the collapse of the peaks characteristic of the crystalline state, to give three small angle reflections in the mesophase indexed as (hk) = (10), (11), (20) (squared spacing ratios $h^2 + k^2 + hk = 1, 3, 4$), confirming the formation of a hexagonal columnar arrangement (Col_h, planar groups $p6$ or $p6mm$). The unit cell parameter varies from $a = 41.1$ Å (30 °C) to $a = 42.6$ Å (60 °C, average 41.9 Å), thus leading to a cross-sectional area $S = 1517$ Å^2 (Table S13). Comparison with the estimated total length of the ligand in its fully extended conformation ($d = 57$ Å) implies significant interdigitation and/or folding of the molten chains. The broad diffraction peak centered around 4.5 Å can be assigned to the molten alkyl chains,[9] but no specific peak arising from a regular packing of the molecules along the columnar axis is observed. To reconcile (i) the well-established crosshatched conformation of the rigid core, (ii) the pseudo-orthogonality of the intermolecular π-stacking found in the crystal structures of $\mathbf{L10}^{Cn}$, and (iii) the formation of a columnar mesophase, we propose that the planes of the gallic ester residues are oriented orthogonal to the column axis, while the planes of the tridentate binding units are parallel (Figure S18). According to the crystal structures of $\mathbf{L10}^{Cn}$, the minimum thickness of a single slice is approximately $h \approx 6$ Å, and the associated volume of the unit cell can be estimated: $V = S \cdot h = 9102$ Å^3. Taking into account a realistic density of $d \approx 1$ g·cm^{-3} in the mesophase,[18] we calculate that the number of molecules per unit cell amounts to $Z = 3.2 \approx 3$ (eq 5, N_{Av} is Avogadro's number, MM_m is the molecular weight of the molecule in g·mol^{-1}, and V is the volume of the unit cell in Å^3).[18]

$$Z = (d \cdot N_{Av} \cdot V \cdot 10^{-24})/MM_m \qquad (5)$$

Three ligands are on average thus packed within each unit cell with a head-to-tail arrangement of the π-stacked tridentate binding units (Figure S18). This produces a rough disklike arrangement of the six gallic esters groups compatible with columnar organization. The irregular and partial interdigitation

Table 2. Phase-Transition Temperatures and Enthalpy and Entropy Changes for the Ligands $\mathbf{L10}^{Cn}$ ($n = 1, 2, 3, 4, 8, 12$) and $\mathbf{L12}^{C12}$

compound	transition[a]	T/°C	ΔH/kJ·mol^{-1}	ΔS/J·mol^{-1}·K^{-1}
$\mathbf{L10}^{C1}$	$Cr_1 \rightarrow Cr_2$	92	*b*	*b*
	$Cr_2 \rightarrow I$	130	*b*	*b*
$\mathbf{L10}^{C2}$	$Cr_1 \rightarrow Cr_2$	65	*b*	*b*
	$Cr_2 \rightarrow Cr_3$	95	*b*	*b*
	$Cr_3 \rightarrow Cr_4$	110	−5.6[c]	−15[c]
	$Cr_4 \rightarrow Cr_5$	144	7.8	19
	$Cr_5 \rightarrow I$	175	12.1	27
$\mathbf{L10}^{C3}$	$Cr_1 \rightarrow Cr_2$	50	*b*	*b*
	$Cr_2 \rightarrow I$	83	*b*	*b*
$\mathbf{L10}^{C4}$	$Cr_1 \rightarrow Cr_2$	87	−21.8[c]	−61[c]
	$Cr_2 \rightarrow I$	118	21.8	56
$\mathbf{L10}^{C8}$	$Cr \rightarrow I$	16	*b*	*b*
$\mathbf{L10}^{C12}$	$Cr_1 \rightarrow Cr_2$	0	*b*	*b*
	$Cr_2 \rightarrow Col_h$	25	*b*	*b*
	$Col_h \rightarrow I$	61	3.3	10
$\mathbf{L12}^{C12}$	$Cr \rightarrow I$	58	31.5	95

[a] Cr = crystal, Col_h = hexagonal columnar phase, I = isotropic fluid. First-order transition temperatures are given as the onset of the peak observed during the second heating processes (Seiko DSC 220C differential scanning calorimeter, 5 °C·min^{-1}, under N_2); the liquid crystalline phases were identified from their optical textures and from SA-XRD studies. [b] Glass transition determined by polarizing light microscopy (PLM). [c] Cold crystallization.

Table 3. Phase-Transition Temperatures for the Complexes [Ln(**L10**^{C12})$(NO_3)_3$] and [Ln(**L12**^{C12})$(NO_3)_3$]

compound	transition[a]	*T*/°C	compound	transition[a]	*T*/°C
[Pr(**L10**^{C12})$(NO_3)_3$]	g → M	125[b]	[Pr(**L12**^{C12})$(NO_3)_3$]	g → M	100[b]
	M → Cub	175[b]		M → Cub	140[b]
	Cub → Dec	249		Cub → Dec	190
[Nd(**L10**^{C12})$(NO_3)_3$]	g → M	70[b]	[Nd(**L12**^{C12})$(NO_3)_3$]	g → M	120[b]
	M → Cub	140[b]		M → Cub	160[b]
	Cub → Dec	211		Cub → Dec	180
[Sm(**L10**^{C12})$(NO_3)_3$]	g → Cub	130[b]	[Sm(**L12**^{C12})$(NO_3)_3$]	g → M	160[b]
	Cub → Dec	180		M → Cub	180[b]
				Cub → Dec	190
[Eu(**L10**^{C12})$(NO_3)_3$]	g → Cub	140[b]	[Eu(**L12**^{C12})$(NO_3)_3$]	g → M	120[b]
	Cub → Dec	>200		M → Cub	180[b]
				Cub → Dec	190
[Gd(**L10**^{C12})$(NO_3)_3$]	g → Cub	145[b]	[Gd(**L12**^{C12})$(NO_3)_3$]	g → M	100[b]
	Cub → Dec	>200		M → Cub	160[b]
				Cub → Dec	190
[Tb(**L10**^{C12})$(NO_3)_3$]	g → Cub	155[b]	[Tb(**L12**^{C12})$(NO_3)_3$]	g → Cub	160[b]
	Cub → Dec	205		Cub → Dec	171
[Dy(**L10**^{C12})$(NO_3)_3$]	g → Cub	155[b]	[Dy(**L12**^{C12})$(NO_3)_3$]	g → M	90[b]
	Cub → Dec	212		M → Dec	180
[Ho(**L10**^{C12})$(NO_3)_3$]	g → Cub	155[b]	[Ho(**L12**^{C12})$(NO_3)_3$]	g → Cub	160[b]
	Cub → Dec	217		Cub → Dec	175
[Er(**L10**^{C12})$(NO_3)_3$]	g → Col_h	160[b]	[Er(**L12**^{C12})$(NO_3)_3$]	g → Col_h	150[b]
	Col_h → Dec	221		Col_h → Cub	180[b]
				Cub → Dec	185
[Tm(**L10**^{C12})$(NO_3)_3$]	g → Col_h	160[b]	[Tm(**L12**^{C12})$(NO_3)_3$]	g → M	160[b]
	Col_h → Dec	221		M → Dec	180
[Yb(**L10**^{C12})$(NO_3)_3$]	g → Col_h	160[b]	[Yb(**L12**^{C12})$(NO_3)_3$]	g → Col_h	175[b]
	Col_h → Dec	223		Col_h → Dec	195
[Lu(**L10**^{C12})$(NO_3)_3$]	g → Col_h	160[b]	[Lu(**L12**^{C12})$(NO_3)_3$]	g → Col_h	155[b]
	Col_h → Dec	223		Col_h → I	190
				I → Dec	195

[a] Cr = crystal, Col_h = hexagonal columnar phase, Cub = cubic phase, g = glass, M = lamello-columnar phase, I = isotropic fluid, Dec = decomposition. Transition temperatures are obtained by PLM, DSC and SA-XRD measurements and given for the second heating processes; the liquid crystalline phases were identified from their optical textures and from SA-XRD studies. [b] Glass transition determined by PLM.

of the tridentate binding units, belonging to different unit cells, along the columnar axis may explain the lack of well-defined structural correlations between the layers. Interestingly, the isomeric bent ligand **L12**^{C12} shows no mesomorphism and isotropizes at 58 °C (Table 2). This behavior is reminiscent of the well-established phenomenological reluctance of bent derivatives possessing a 2,6-bis(benzimidazole)pyridine cores for producing thermotropic liquid crystalline phases (only **L9** has been shown to produce a Col_r mesophase over 8 °C).[17] In this context, it is remarkable that the complexes [Ln(**L10**^{C12})-$(NO_3)_3$] (Ln = Pr−Lu),[34] in which the tricoordinated cis−cis ligands are indeed bent, display liquid crystalline behavior at high temperature (Table 3). A thorough combination of thermogravimetric (TG), DSC, and IR analyses shows that (i) the interstitial water molecules (Table S1) are lost around 60−70 °C before the melting processes, (ii) these complexes are stable over several heating−cooling cycles provided that the isotropization temperature is not reached, (iii) the melting processes systematically correspond to glass transitions (Table 3), and (iv) the isotropization process is accompanied by a fast exothermic decomposition resulting from the oxidation of the organic matrix by nitrate anions at high temperature in the isotropic liquid.[15−17] The phase transitions accompanying the melting processes can be unambiguously detected by PLM and further confirmed by SA-XRD measurements (Table S13). For the smallest lanthanides (Ln = Er−Lu), the birefringent textures (Figure S19a) observed for the monometallic complexes [Ln(**L10**^{C12})$(NO_3)_3$] in the mesophases (160−223 °C, Table 3), combined with the detection of up to seven fine reflections in the SA-XRD patterns (Figure 7a, squared spacing ratios $h^2 + k^2 + hk$ = 1, 3, 4, 7, 9, 12, 13 with (hk) = (10), (11), (20), (21), (30), (22), (31)) indicate the formation of a well-correlated hexagonal columnar arrangement (Col_h, plane group *p*6 or *p*6*mm*).[9,18]

The mathematical analysis leads to a rather short intercolumn separation in the range a = 31.2−31.9 Å, with associated cross-sectional areas of S = 842−876 Å^2 (Table S13). The observation of a single diffuse band at 4.5 Å (Figure 7a), characteristic of the molten alkyl chains, suggests a poor structural correlation between the slices along the columns, as previously discussed for the free ligand. Taking a typical stacking period of approximately $h \approx 4.5$ Å between two packed tridentate aromatic binding units within the column (i.e., the associated broad peak could be masked by the one of the molten chains)[18] and a density of $d = 1$ g·cm^{-3} in the Col_h mesophases, we calculate $Z = 1.1 \approx 1$ molecule per unit cell (eq 5). Therefore, a single elliptic hemi-disklike complex [Ln(**L10**^{C12})$(NO_3)_3$] (Ln = Er−Lu) occupies the cross section of one column, or two complexes occupy a columnar section 9 Å high (Figure 8a). This assumption has been checked by a molecular dynamics simulation of a hexagonal cell containing two molecules disposed in head-to-tail orientation and that are 9 Å in height, the other dimensions being set from the experimental cross section of the column. The calculation shows that the space is well filled with the aliphatic chains, with a density of 0.92, and that the molecules adopt a tilted position from the columnar axis. From the crystal structure of [Yb(**L10**^{C0})$(NO_3)_3$] (**9**), one can reasonably estimate that the length of the coordinated bent ligand

(34) The complexes [Ln(**L***i*^{C12})$(NO_3)_3$] (*i* = 10, 12; Ln = La, Ce) display thermal behavior close to that described for Ln = Pr and Nd, but their reproducibility is doubtful and these complexes are not further considered.

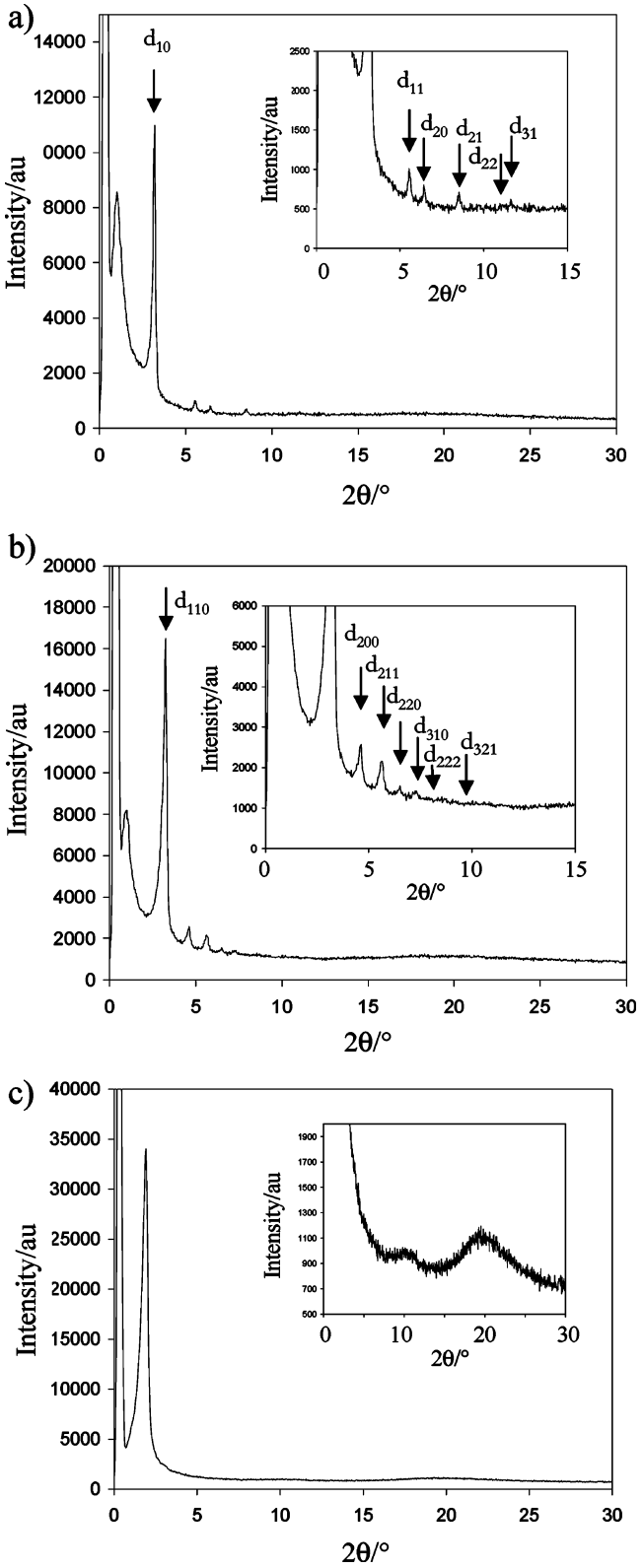

Figure 7. SA-XRD profiles in the liquid crystalline phases and associated indexations for (a) [Lu(**L10**^{C12})$(NO_3)_3$] at 200 °C, (b) [Dy(**L10**^{C12})$(NO_3)_3$] at 200 °C, and (c) [Nd(**L10**^{C12})$(NO_3)_3$] at 80 °C.

strand in its extended form in [Ln(**L10**^{C12})$(NO_3)_3$] amounts to L ≈ 45 Å, while the perpendicular expansion of the complex is smaller (about 35 Å, Figure 8a).[18] The long axis of the ellipse (45 Å) is significantly longer than the intercolumnar separation (32 Å), which implies a significant interdigitation and/or folding of the molten chains and a tilt of the slices within the column. Since the coordination of the bulky Ln$(NO_3)_3$ metallic unit restricts intermolecular π-stacking between the coordinated tridentate units to a partial overlap between the central pyridine rings, we propose that the complexes in one column adopt head-to-tail orientations for ensuring (i) weak intracolumnar packing and (ii) pseudo-circular spreading of the flexible chains (Figure 8b),[35] as previously reported for [M(**L11**)Cl_2] (M = Mn, Co, Ni, Zn).[19]

For the midrange lanthanides, homeotropic textures are observed by PLM for the complexes [Ln(**L10**^{C12})$(NO_3)_3$] (Ln = Sm−Ho) in the temperature range 130−212 °C (Table 3). Application of pressure on the sample induces bright orthorhombic flashes in the texture, which suggests the formation of a viscous cubic mesophase (Figure S19b).[8,9] This is confirmed by SA-XRD profiles displaying a set of up to nine fine reflections for which the reciprocal spacings are in the ratio $\sqrt{h^2+k^2+l^2}$ = 1, $\sqrt{2}$, $\sqrt{3}$, $\sqrt{4}$, $\sqrt{5}$, $\sqrt{6}$, $\sqrt{7}$, $\sqrt{8}$, and $\sqrt{9}$ (Figure 7b) compatible with a body-centered cubic lattice (a = 37.3−38.3 Å, V = 51951−56244 Å^3, Table S13) since the presence of the reflection corresponding to the ratio $\sqrt{7}$ permits the immediate elimination of any primitive (*P*-Bravais type) and face-centered (*F*-Bravais type) space groups. For a body-centered cubic lattice (*I*-type), the considered sequence in this case is: $\sqrt{2}$, $\sqrt{4}$, $\sqrt{6}$, $\sqrt{8}$, $\sqrt{10}$, $\sqrt{12}$, $\sqrt{14}$, $\sqrt{16}$, $\sqrt{18}$, and the reflections can be indexed as (110), (200), (211), (220), (310), (222), (321), (400), and (411/330). Among the 10 cubic-centered groups, the four space groups $Ia\bar{3}$, $I4_132$, $I\bar{4}3d$, and $Ia\bar{3}d$ can be disregarded because of the presence of forbidden reflections not allowed by the general conditions.[36] We are left with six equiprobable groups (they all have the same general conditions of extinction), which are $I23$, $I2_13$, $Im\bar{3}$, $I432$, $I\bar{4}3m$, and $Im\bar{3}m$. The use of eq 5 with $d \approx 1$ gives $Z = 16$ complexes per unit cell, which is in line with the 16 general or special Wykoff positions found in the space group $Im\bar{3}m$.[18] Thus, by analogy with all known cubic space groups discovered in thermotropic liquid crystals,[8b,37] the most probable one, and the one we will consider thereafter, is the $Im\bar{3}m$ space group (No. 229). It is, however, impossible at this stage to discriminate between a micellar (Figure S20a) or a bicontinuous (Figure S20b,c) structure for this type of cubic phase. From a molecular point of view, the larger metallic cores provided by the midrange lanthanides in [Ln(**L10**^{C12})$(NO_3)_3$] (Ln = Sm−Ho) are still compatible with the exclusive formation of monometallic complexes (i.e., the crystal structure of [Eu(**L10**^{C0})$(NO_3)_3(CH_3CN)$] is monomeric (**8**), and the ^{1}H NMR data show [Eu(**L10**^{C12})-$(NO_3)_3$] to be the major species in solution). However, the intracolumnar interactions involving the coordinated tridentate binding units are significantly weakened by the increasing size of the metallic Ln$(NO_3)_3$ cores (Figure 8b). As a consequence, the flexibility within each column increases, which eventually allows larger oscillations (undulating columnar cores model).[9a]

(35) (a) Lai, C. K.; Serrette, A. G.; Swager, T. M. *J. Am. Chem. Soc.* **1992**, *114*, 7948−7949. (b) Zheng, H.; Lai, C. K.; Swager, T. M. *Chem. Mater.* **1994**, *6*, 101−103. (c) Coco, S.; Diez-Esposito, F.; Espinet, P.; Fernandez-Mayordomo, C.; Martin-Alvarez, J. M.; Levelut, A.-M. *Chem. Mater.* **1998**, *10*, 3666−3671.

(36) *International Tables for Crystallography*, 4th ed.; Hahn, T., Ed.; The International Union of Crystallography by Kluwer Academic Publishers: Dordrecht, The Netherlands, Boston, London, 1995; Vol. A.

(37) Diele, S.; Göring, P. In *Handbook of Liquid Crystals*; Demus, D., Goodby, J. W., Gray, G. W., Spiess, H. W., Vill, V., Eds.; Wiley-VCH: Weinheim, Germany, 1998; Vol. 2B, Chapter XIII, pp 887−900.

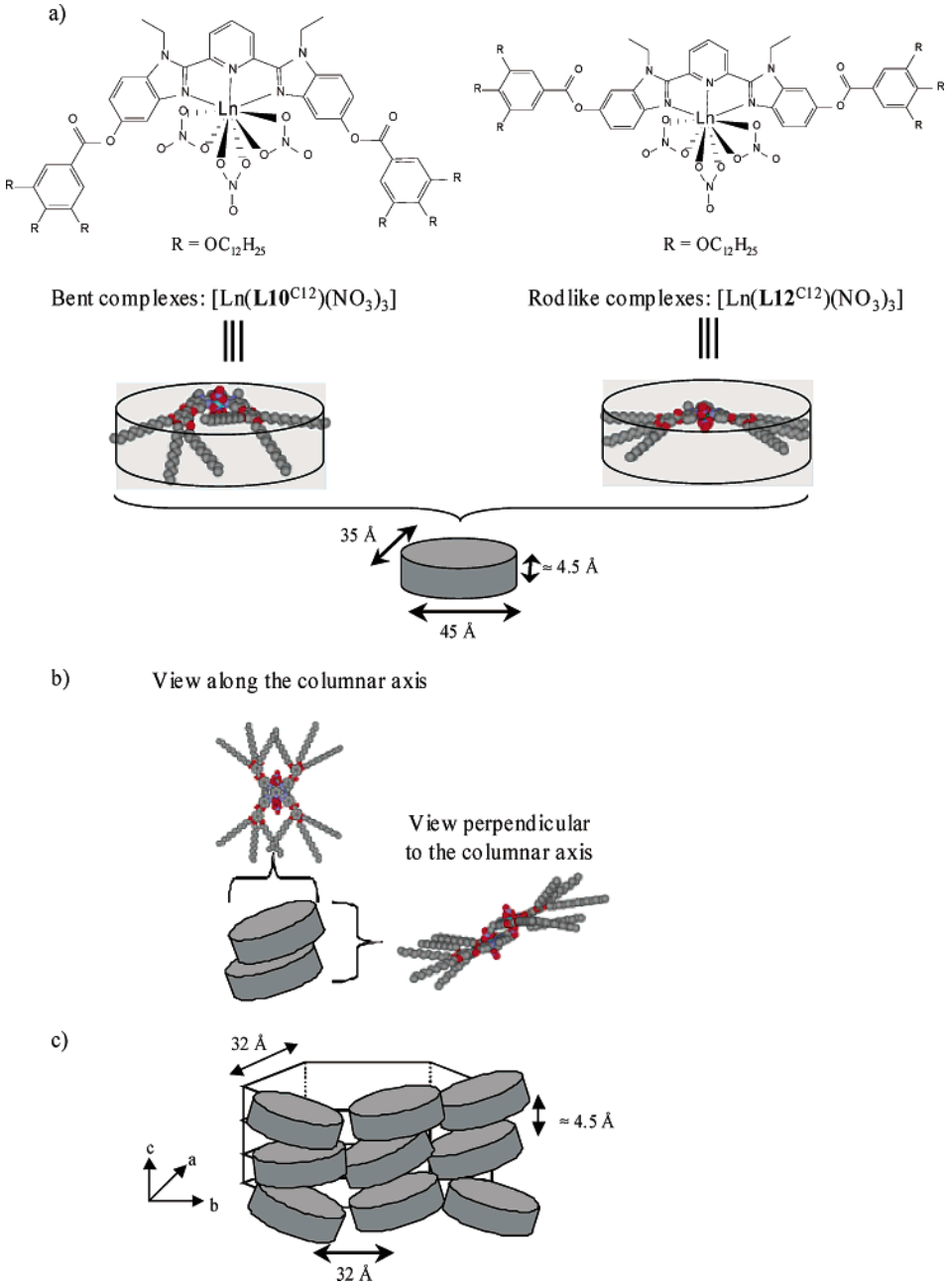

Figure 8. Molecular modeling of [Ln(**Li**^{C12})$(NO_3)_3$] (i = 10, Ln = Er−Lu, and i = 12, Ln = Yb−Lu) in the Col_h mesophase. Schematic representations of (a) the unit cells, (b) the head-to-tail packing of two adjacent cells within a column, and (c) the arrangement of the columns within the hexagonal lattice.

This mechanism, combined with the occurrence of competitive intercolumnar interactions involving the peripheral gallic esters, produces point dislocations that may be responsible for the formation of the cubic mesophase (Figure S20).[8b]

The thermal behavior of [Ln(**L10**^{C12})$(NO_3)_3$] with the larger lanthanides Ln = Pr and Nd is quite different. The melting process leads to a birefringent mesophase (temperature range 70−175 °C, Table 3 and Figure S19c), which displays one sharp reflection at d = 44.0−50.2 Å and two broad reflections at 8.5−8.8 and 4.5 Å (molten alkyl chains, Figure 7c). At higher temperatures, this mesophase is transformed into the Cub phase previously detected with the analogous midrange lanthanides (a = 38.2 Å, Table S13). According to the crystal structure of [Eu_2(**L12**^{C0})$_2(NO_3)_6$] (**10**), we expect that the dimerization process, occurring for large Ln(III), assembles two monometallic units [Ln(**L10**^{C12})$(NO_3)_3$] (Figure 8) to give the rodlike bimetallic complexes [Ln_2(**L10**^{C12})$_2(NO_3)_6$] (Figure 9). Since the locations of the 12 alkyl chains are not strictly perpendicular or parallel to the axis of the cylinder, a columnar packing is destabilized, and a less organized lamellar arrangement can be postulated. Such a lamellar organization is supported by the calculation of the molecular areas S = 75−85 Å^2 (Table S13), which correspond to approximately three times the cross section of one chain for a monomer,[38] in agreement with the cylindrical arrangement proposed in Figure 9. Moreover, the average interlayer separation amounts to ∼44−50 Å, which compares well with the total length of the coordinated bent ligand **L10**^{C12} in its elongated form (d = 45 Å).[18] Finally, some residual

(38) Doolitle, K. J. *J. Appl. Phys.* **1951**, *22*, 1471−1479.

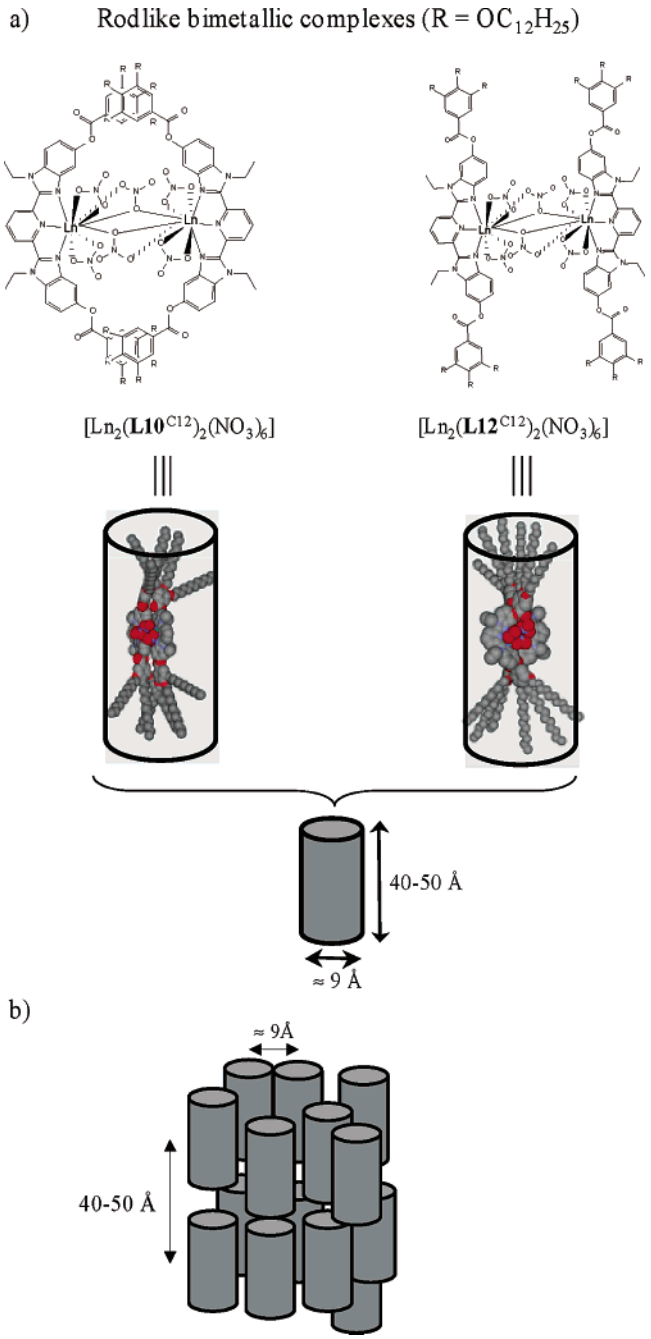

Figure 9. Molecular modeling of [Ln_2(**L*i***^{C12})$_2$(NO_3)$_6$] (i = 10, Ln = Pr−Nd and i = 12, Ln = Pr−Tm) in the lamello-columnar mesophase. Schematic representations of (a) the rodlike bimetallic complexes and (b) the macroscopic ordering in the 3D-lattice.

positional ordering within each layer, reminiscent from a columnar arrangement, is compatible with the broad peak detected around 8.5−8.8 Å (Figure 9). This postulated lamello-columnar arrangement (L_{Col}) is only found for the larger Ln(III) because of their higher propensity to form dimers at low temperature. If the large negative entropy of the dimerization process, demonstrated in absence of solvation by ^{1}H NMR in CD_2Cl_2, also holds in the liquid crystalline phase, dissociation into monometallic complexes is expected at higher temperature with the formation of the cubic phase, a sequence which is indeed systematically observed experimentally.

Our interpretation of the dependence of the mesomorphism on the lanthanide size is further supported by the thermal

Chart 2

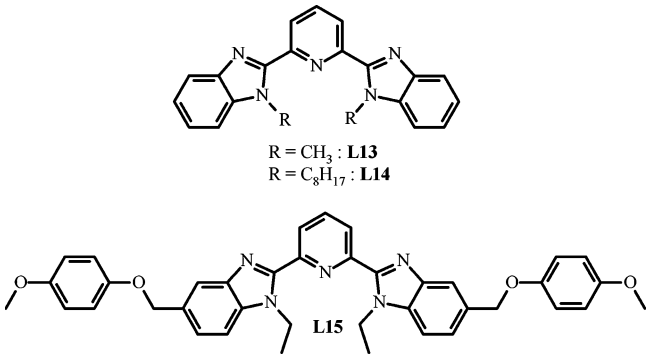

behavior of the isomeric complexes [Ln(**L12**^{C12})(NO_3)$_3$]. Again, thorough combination of TG, DSC, and IR analyses similarly shows that (i) the interstitial water molecules are lost prior to the melting processes, (ii) the complexes are stable over several heating−cooling cycles, provided that the isotropization temperature is not reached, and (iii) the melting processes systematically correspond to glass transitions (Table 3). We note that the decomposition occurs at lower temperatures (ΔT = 30−40 °C) when compared with the analogous complexes [Ln(**L10**^{C12})-(NO_3)$_3$] (Table 3). The PLM and SA-XRD studies show the formation of very similar organizations in the mesophases with a smooth evolution from hexagonal columnar (Col_h) for the smallest Ln(III) (Lu, Yb, Figure 8 and Table 3) toward a cubic phase (Cub) for midrange Ln(III) (Er−Tb, Figure S20 and Table 3), and finally lamello-columnar (L_{Col}) followed by Cub phases for the larger Ln(III) (Pr−Gd, Figure 9 and Table 3). A remarkable difference concerns the detection of the lamello-columnar mesophases along a considerable part of the lanthanide series for [Ln(**L12**^{C12})(NO_3)$_3$] (Pr−Tm), whereas this arrangement is only found for Pr and Nd in [Ln(**L10**^{C12})(NO_3)$_3$] (Table S14). This can be ascribed to the larger propensity of [Ln(**L12**^{C12})(NO_3)$_3$] to dimerize because the approach of two rodlike complexes is more favorable. This is shown by the thermodynamic data obtained for the complexes [Eu(**L*i***^{C12})-(NO_3)$_3$] (i = 10, 12) in CD_2Cl_2. From the collected enthalpic and entropic contributions for these complexes, the critical temperatures for which $K_d^{Ln-Li} = 1$ (equilibrium 1) amount to $T_c = \Delta H_d^{Eu-L10^{C12}}/\Delta S_d^{Eu-L10^{C12}}$ = 334(39) K and $T_c = \Delta H_d^{Eu-L12^{C12}}/\Delta S_d^{Eu-L12^{C12}}$ = 542(96) K. In other words, T_c is the temperature at which each compound exists as a 1:1 mixture of monomer ([Ln(**L*i***^{C12})(NO_3)$_3$]) and dimer ([Ln_2(**L*i***^{C12})$_2$-(NO_3)$_6$]) in solution, when the total concentration of ligand amounts to 3 mol·dm^{-3}. Above this temperature, the monometallic complex dominates, and we conclude that the probability to isolate the dimer by crystallization at room temperature is larger with **L12**^{C12}, in agreement with the rather systematic detection of lamello-columnar phases at "low" temperatures for [Ln(**L12**^{C12})(NO_3)$_3$] (Table S14). Please note that the density of $d \approx 1$ g·cm^{-3} considered in the mesophases approximately corresponds to a concentration of 0.5 mol·dm^{-3} in [Ln(**L*i***^{C12})-(NO_3)$_3$], which is of comparable magnitude as that used for the interpretation of T_c.

Detecting Phase Transitions in Cubic and Columnar Liquid Crystals by Lanthanide-Centered Luminescence. The strong red europium-centered photoluminescence evidenced in the nonlipophilic model complexes [Eu(**L*i***)(NO_3)$_3$] (i = 13, 14, Chart 2)[23,25] can be exploited for extracting thermal and

structural information on the melting process.[22,39,40] As a first step toward this goal, the bent complex [Eu(**L10**^{C12})$(NO_3)_3$] has been investigated at 10 and 295 K with high-resolution laser-excited luminescence to probe the metal ion environment. We focus here on the three following points that are crucial in the field of luminescent liquid crystals and phase transitions. (1) The excitation profile of the nondegenerate Eu($^5D_0 \leftarrow {}^7F_0$) transition in [Eu(**L10**^{C12})$(NO_3)_3$] shows one narrow symmetrical component at both 10 K (17 215 cm^{-1}, full width at half-height, fwhh = 3.0 cm^{-1}) and 295 K (17 226 cm^{-1}, fwhh = 7.8 cm^{-1}, Figure S21a), which is diagnostic for the existence of a single metallic environment in the microcrystalline sample, very similar to that found in the monometallic nine-coordinate model complex [Eu(**L14**)$(NO_3)_3$] (17 226 cm^{-1} at 295 K),[23] for which the X-ray crystal structure has been solved.[25] (2) Upon selective excitation, the europium-centered emission spectrum is dominated by the hypersensitive electric dipolar $^5D_0 \rightarrow {}^7F_2$ transition, while the magnetic dipolar transition $^5D_0 \rightarrow {}^7F_1$ is split into $2J + 1 = 3$ components (Figure S21b). These features imply a low symmetry around Eu(III) in [Eu(**L10**^{C12})$(NO_3)_3$], as found in the crystal structure of the complex [Eu(**L14**)$(NO_3)_3$].[25] (3) The Eu($^5D_0$) luminescence decay is a single exponential, and the corresponding lifetime amounts to $\tau = 1.29-1.25$ ms between 10 and 295 K. This minor temperature dependence points to an efficient protection of the metallic center from coupling with high-energy oscillators. Moreover, the close match with $\tau = 1.15-1.11$ ms reported for [Eu(**L14**)$(NO_3)_3$] (between 4 and 295 K)[25] eventually demonstrates that a very similar nine-coordinate environment holds in [Eu(**L10**^{C12})$(NO_3)_3$], which contrasts with the 10-coordinate site exhibited in the less-protected [Eu(**L10**^{C0})$(NO_3)_3(CH_3CN)$] complex (**8**). From a theoretical point of view, the temperature-dependent deactivation processes should result in an overall decrease of the emission intensity (I_{obs}) and associated lifetime (τ_{obs}), varying as the exponential function $y = y_0 \cdot \exp(-C/RT)$.[41] Therefore, plots of $\ln(I_{obs}/I_{295K})$ or $\ln(\tau_{obs}/\tau_{295K})$ versus the inverse of the absolute temperature (T^{-1}) should be linear as long as no first-order phase transition occurs.[39,40] However, sigmoid variation is seen for both logarithmic plots, when [Eu(**L10**^{C12})$(NO_3)_3$] enters its cubic mesophase during the first heating process (Figure 10). Since the contribution due to the concomitant change in the refractive index is weak compared with the large coupling between the phonon density of states and the ^5D_J electronic states induced in the less ordered mesophase,[39] the sigmoid curve can be traced back to minor structural changes induced by the Cr → Cub melting process. A mathematical analysis gives $T = 413(2)$ K (i.e., 140(2) °C) for the transition temperature, which exactly matches that found by PLM and SA-XRD (140 °C, Table 3). Interestingly, the first heating process displays a first-order transition Cr → Cub (Figure 10a), which strongly depends on the conditions used during the original isolation of the complex in the solid state. The following cooling process and subsequent heating/cooling cycles show that the organization in the Cub mesophase is supercooled in the final glassy state (Figure 10a). Since no significant structural variation occurs during the subsequent phase transition, we do not expect major deviations

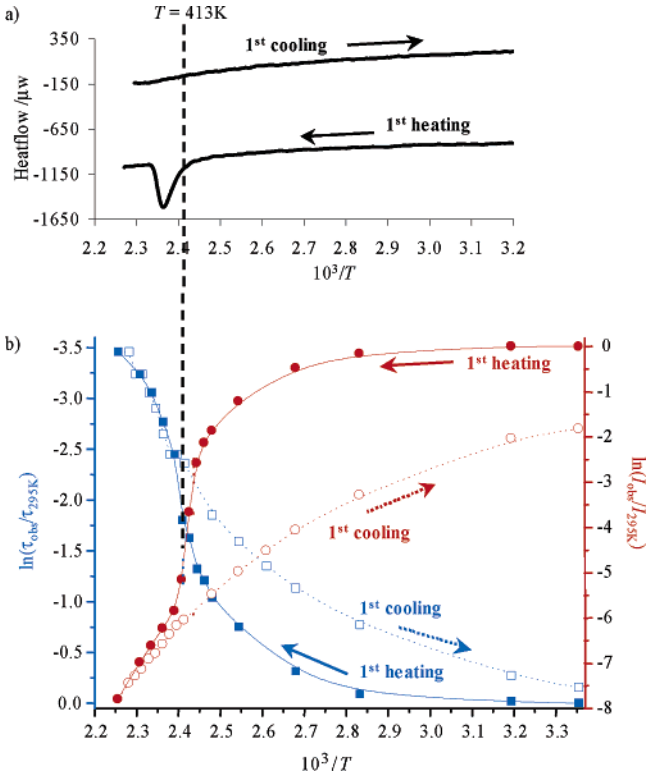

Figure 10. (a) DSC traces and (b) plots of $\ln(I_{obs}/I_{295K})$ (red) and $\ln(\tau_{obs}/\tau_{295K})$ (blue) versus the inverse of the absolute temperature (T^{-1}) obtained during the first heating/cooling cycle in [Eu(**L10**^{C12})$(NO_3)_3$].

from linearity for the plots of $\ln(I_{obs}/I_{295K})$ or $\ln(\tau_{obs}/\tau_{295K})$ versus T^{-1}, as it is highlighted in Figure 10b during the first cooling process. The minor residual curvature can be assigned to the faint nonlinear contribution of the refractive index.[40] In other words, the different macroscopic organizations characterizing the original microcrystals and the Cub mesophase can be probed by luminescence thanks to the associated minor structural variations induced at the molecular level. However, glass transitions are not accessible. Unfortunately, the signals observed for the europium-centered emission at high temperature are too broad to allow a detailed crystal-field analysis of the geometrical changes in the coordination sphere induced by the phase transition.

This sensitive luminescent technique has been further exploited for probing the Cr → Col_h transitions occurring with small lanthanides. The doped complex [$Lu_{0.95}Eu_{0.05}$(**L10**^{C12})$(NO_3)_3$] displays the same melting process (g $\xrightarrow{160°C}$ Col_h) as that found in the pure Lu complex (Table 3). The emission spectrum (Figure S22) and the Eu($^5D_0$) lifetime in the solid state ($\tau_{10-295K} = 1.29-1.22$ ms) are typical of the low-symmetrical nine-coordinate metallic center found in [Eu(**L10**^{C12})$(NO_3)_3$]. Plots of $\ln(I_{obs}/I_{295K})$ or $\ln(\tau_{obs}/\tau_{295K})$ versus T^{-1} indeed show sigmoid curves during the first heating, with $T = 161(2)$ °C in very good agreement with PLM measurements (Figure S23). Again, the cooling process and subsequent heating/cooling cycles only display the glass transition that escapes detection by DSC and luminescence.

Conclusion

The ligands **L10**^{Cn} and **L12**^{Cn} are ideally suited for exploring the consequences of specific molecular shapes and charge distributions on the intermolecular interactions responsible for

(39) Suarez, S.; Imbert, D.; Gumy, F.; Piguet, C.; Bünzli, J.-C. G. *Chem. Mater.* **2004**, *16*, 3257−3266.
(40) Driesen, K.; Binnemans, K. *Liq. Cryst.* **2004**, *31*, 601−605.
(41) (a) Kleinerman, M.; Choi, S.-I. *J. Chem. Phys.* **1968**, *49*, 3901−3910. (b) Hüfner, S. *Optical Spectra of Transparent Rare Earth Compounds*; Academic Press: New York, 1978.

the macroscopic organization. In these systems, (i) the global anisometry (rodlike versus bent) of the ligand can be modulated by the judicious connection of the semirigid lipophilic sidearms at the 5,5′- or 6,6′-positions of the benzimidazole rings, (ii) the rodlike ⇌ bent interconversion process can be induced by simple complexation to metal ions, (iii) the carboxylate spacers fix the two gallic esters residues roughly perpendicular to the tridentate binding unit, thus providing two predictable directions for intermolecular π-stacking, and (iv) the gallic esters possess three divergent lipophilic alkoxy chains, which increases the volume ratio *V*(alkyl chain)/*V*(rigid core) and favors thermotropic mesomorphism.[7−9] This versatility is completed by the minor, but significant, structural changes associated with the lanthanide contraction. For the lighter (i.e., the larger) lanthanides, the trend for 10-coordination favors the formation of the bimetallic rodlike nitrato-bridged dimers $[Ln_2(\mathbf{L}i^{Cn})_2(NO_3)_6]$, but dissociation yielding the monometallic hemi-disklike complexes $[Ln(\mathbf{L}i^{Cn})(NO_3)_3]$ with the smaller Ln(III) dominates the solid state and solution structures. This crucial variation of the microscopic arrangement, combined with the tuning of the specific anisometry of the ligand $\mathbf{L}i^{C12}$ ($i = 10, 12$), provides a complete library of molecular shapes. Moreover, the predetermined orthogonal directions for intermolecular π-stacking allows a rational amplification of the molecular organization to program macroscopic order in the liquid crystalline phases. For the smaller Ln(III), the hemi-disklike monometallic complexes $[Ln(\mathbf{L}i^{C12})(NO_3)_3]$ are compact enough to induce intermolecular pyridine−pyridine interactions between head-to-tail tridentate cores, which are responsible for the formation of columns in hexagonal lattices. When the ionic radius increases in the monometallic complexes $[Ln(\mathbf{L}i^{C12})(NO_3)_3]$ (i.e., for midrange Ln(III)), the intracolumnar interactions weaken. Orthogonal intercolumnar packing occurring between the peripheral gallic ester residues competes with intracolumnar packing, thus leading to the oscillation of the columns. Dislocation results, and a body-centered cubic phase Cub is formed.[8,9] Finally, the existence of rodlike dimers $[Ln_2(\mathbf{L}i^{Cn})_2(NO_3)_6]$ with the larger Ln(III) removes strong intermolecular π-stacking, and a residual lamellar ordering is detected. In the absence of coordinating solvent, the considerable entropic cost of the dimerization process is expected to control the free energy at high temperature, and the lamello-columnar phase (induced by the dimeric bimetallic building blocks) is indeed transformed upon heating into the cubic phase (induced by the monometallic building blocks). The concomitant detection of anomalous luminescence behavior occurring during first-order phase transitions is also encouraging for implementing new optical functions in liquid crystalline displays.[21c,42]

Acknowledgment. We thank H. Lartigue, S. Schweizer, B. Bocquet, and F. Gumy for their technical assistance. Financial support from the Swiss National Science Foundation, National Research Program 47 "Supramolecular Functional Materials" is gratefully acknowledged.

Supporting Information Available: The Experimental Section and the associated analytical data. Additional tables (Tables S1−S15) and figures (Figures S1−S24) for structural and spectroscopic analyses and crystallographic data for compounds **5−11** in CIF formats. This material is available free of charge via the Internet at http://pubs.acs.org.

JA0446101

(42) (a) Weder, C.; Sarwa, C.; Montali, A.; Bastiaansen, C.; Smith, P. *Science* **1998**, *279*, 835−837. (b) Sato, Y.; Takahashi, N.; Sato, S. *Jpn. J. Appl. Phys.* **1998**, *37*, L129−L130. (c) Yamaguchi, R.; Ito, Y.; Sato, Y.; Sato, S. *Mol. Cryst. Liq. Cryst. A* **1999**, *331*, 2417−2422.